Received: Added at production | Revised: Added at production | Accepted: Added at production

DOI: xxx/xxxx

ARTICLE TYPE

# Computational fluid dynamics of blood flow in an idealized left human heart

Luca Dedè*[1] | Filippo Menghini[2] | Alfio Quarteroni[1,3]

[1]MOX–Mathematics Department, Politecnico di Milano, Italy
[2]Institute of Mathematics, École Polytechnique Fédérale de Lausanne, Switzerland
[3]Institute of Mathematics, École Polytechnique Fédérale de Lausanne, Switzerland (Honorary Professor)

**Correspondence**
* Luca Dedè, MOX–Mathematics Deptartment, Politecnico di Milano, Piazza Leonardo da Vinci 32, 20133 Milano, Italy.
Email: luca.dede@polimi.it

**Summary**

We construct a idealized computational model of the left human heart for the study of the blood flow dynamics in the left atrium and ventricle. We solve the Navier-Stokes equations in the ALE formulation and we prescribe the left heart wall displacement based on physiological data; moreover, we consider the presence of both the mitral and aortic valves through the resistive method. We simulate the left heart hemodynamics by means of the Finite Element method and we consider the Variational Multiscale Large Eddy Simulation (LES) formulation to account for the transitional and nearly turbulent regimes of the blood flow in physiological conditions. The main contribution of this paper is the characterization of the blood flow in an idealized configuration of the left heart aiming at reproducing function in normal conditions; our assessment is based on the analysis of instantaneous and phase averaged velocity fields, blood pressure, and other clinically meaningful fluid dynamics indicators. Finally, we show that our idealized computational model can be suitably used to study and critically discuss pathological scenarios like that of a regurgitant mitral valve.

**KEYWORDS:**
Heart modeling, Computational Fluid Dynamics, Finite Element method, Variational Multiscale method, LES modeling

## 1 | INTRODUCTION

Non-invasive imaging techniques have substantially progressed in recent years and are nowadays widely applied to study the hemodynamics of the heart[1,2,3,4]. In particular, magnetic resonance imaging (MRI) can be used to visualize and register the heart displacement (deformation) and thus determine the blood flow velocity at the endocardium wall. Phase-contrast magnetic resonance imaging (pc–MRI)[5] allows acquiring 4D flow data to be exploited in reconstructing patient–specific the blood velocity field in the heart chambers. This technique requires to be applied to several heart cycles (heartbeats) in order to obtain reliable information on the fluid dynamics quantities of interest that are indeed averaged over different cycles[1,2]. Although yielding a meaningful representation of the blood flow during the heartbeat, these image-based techniques cannot provide yet highly-resolved instantaneous fields and cycle-to-cycle variations. Moreover, detailed characterizations of the blood flow needs to be complemented by other suitable fluid dynamics indicators. For example, Wall Shear Stress and Oscillatory Stress Index are commonly used to assess blood flows in arteries and blood vessels[6]; their use instead for heart chambers can provide a better characterization of the blood flows and help comparing them in physiological or pathological conditions. Echocardiography, which uses sound waves to measure and analyze blood flow velocity in the heart chambers, allows assessing flows through the valves and detecting pathological conditions like a regurgitant mitral valve; however, echocardiography only provides a

partial characterization of the blood flow as it measures one component of the velocity vector, i.e. the one normal to the probe orientation. We refer the reader to [1,2,3,4,5] for an overview of these techniques applied in both physiological and pathological conditions.

In recent years *in-silico* studies have been increasingly applied to study the hemodynamics in the whole cardiovascular system [7,8,9,10,11]. Several works focusing on heart valve dynamics, aneurysm and stenosis formation and growth in arteries, fluid-structure interaction of blood and artery walls, as well as ventricle or heart hemodynamics have been performed with the main focus being the blood flow and its interaction with the surrounding tissue [12,13,14,15,16,17,18,19,20,21,22,23]. Few works have dealt with the cardiovascular system as a closed–loop dynamical system that includes the heart; see e.g. [7,24,25,26] and the references therein. Still, there is a strong interest in performing patient-specific simulations that could potentially help clinicians to assess patient condition and to possibly provide indications for personalized therapies. However, this task requires a significantly large amount of computational resources which could be prohibitive if routinely applied in therapy assessment. To overcome this difficulty, reduced order techniques could be exploited by studying parametric models to explore patient-specific variability; this has the potential to provide valuable information in a consistent, reliable, and computationally less expensive way [27,28]. Towards this goal of personalized medicine, the first step is the construction of a meaningful reference model of the left heart, namely idealized, which is able to represent “normal" conditions. We consider such a computational fluid dynamics model of the left heart as the ground base for further studies of variability with respect to geometric and physical data. As inter-patients variability is a crucial issue to be assessed in personalized medicine, the development of a parametrized model could lead to important achievements towards affordable personalized simulation and therapy. Moreover, an idealized geometry which resembles that of an average adult individual, can provide valuable hints and indications on the function and properties of a normal heart.

In this work, we propose a detailed computational model for the fluid dynamics of the whole left heart, which is comprised of the left atrium and left ventricle, the mitral and aortic valves, the pulmonary veins and the aortic root. Our idealized model is aimed at the characterization of blood flow features in the left chambers in a “normal" heart (with size and conditions in the physiological range) along the whole heartbeat and for several heart cycles. A similar and very detailed study has been proposed in [22] for a real heart of a healthy individual. Instead here we consider an idealized geometry of the left heart, which is meant to be representative of an healthy adult population under physiological conditions. In our study, the endocardium wall displacement is prescribed compatibly with the behavior of the chambers' volume vs. time that is depicted in a typical Wiggers diagram [29]. On the contrary, in [22], the wall motion is acquired from medical images of a healthy individual, thus allowing to characterize only the blood flows in the heart of this specific individual and only in the operating regime during which the images were acquired. Instead, our idealized model easily allows studying blood flows in heart working in conditions that depart from the average Wiggers diagram.

We model the blood flow by means of the incompressible Navier-Stokes equations in the ALE framework and we use the resitive method [12,30,31] to account for the mitral and aortic valves as immersed in the computational fluid domain. Several numerical studies of the blood flow dynamics in the left ventricle alone have been already performed; see e.g. [18,20,32,33,34,35]. However, these hemodynamics studies are significantly affected by the model used to account for the mitral valve. Indeed, blood flows in the diastolic regime of the left ventricle are strongly affected by the mitral valve and left atrium dynamics as widely reported for example in [18,20,36,37] and references therein; just to make an example, accounting for blood inflow in the left ventricle during diastole by means of Dirichlet conditions yields results far from the realistic ones. Instead, modeling the left atrium and ventricle as a single and topologically connected computational domain (the left heart), together with the resistive method for the mitral valve, allows us to circumvent the issue of modeling blood flows entering the left ventricle from the mitral valve orifice.

Blood flow in the heart chamber can reach Reynolds numbers around 5000 in physiological conditions, for which turbulence should be taken into account, in principle. The simulation of a turbulent flow can be based on several approaches. In Direct Numerical Simulations, all the velocity and pressure small scales are numerically solved by using space and time discretizations which are able to fully resolve Kolmogorov lengths. In Large Eddy Simulations (LES) only the largest scales of the solution are directly simulated, whereas the smaller scales are modeled [38,39]. In this respect, the Variational Multiscale (VMS) model represents an alternative way to the widely used Smagorinsky or Germano models in defining a sub-grid model for the LES [40]. As VMS is in fact a stabilization technique for the Navier-Stokes equations, in this work we use the VMS-LES formulation [40] to yield inf-sup stable approximations when considering the same finite element spaces for the velocity and pressure fields, to control numerical oscillations associated to flow regimes at locally large Reynolds numbers, and to model turbulence according to LES principles. Specifically, our numerical model is based on the method proposed in [43], which considers a semi-implicit BDF time discretization and the finite element method for space discretization within the VMS-LES formulation. With respect to [43], we extend the numerical approach to account for the resistive method mimicking the presence of the aortic and mitral

valves within the VMS-LES formulation. As alternative formulation to the VMS-LES one, we use the Streamline Upwind Petrov-Galerkin (SUPG) stabilization method to numerically solve the problem; we also provide a systematic comparison of the numerical results obtained by means of the two methods in terms of fluid dynamics outputs.

We use our computational model of the idealized left heart to assess and characterize the blood flow dynamics in the chambers of our idealized "normal" heart. We purposely use both instantaneous and phase averaged quantities. Moreover, we use several clinically and physically meaningful fluid dynamics indicators as kinetic energy, fluctuating kinetic energy, and enstrophy, other than the Wall Shear Stress, Oscillatory Shear Index and Relative Residence Time. Earlier computational fluid dynamics studies for the left ventricle alone already provided indications that the blood flow regime is transitional and/or nearly turbulent [13,18,20,22]. As highlighted in [22] for an healthy individual, we confirm that also for our idealized "normal" heart fully developed turbulence in the whole heart chambers is not sustained for a significant time lapse during the heartbeat: the flow regime is definitely not laminar, but characterized by complex features, instabilities, and interaction of vortexes at different spatio-temporal scales.

Finally, we use our idealized model, developed to assess blood flows in "normal" conditions in the physiological range, as the starting point to study mitral valve regurgitation; this is harmful pathological condition for which the mitral valve does not fully seal during systole and allows blood to flow backward into the left atrium. In particular, we aim at showing that our model can be straightforwardly used to characterize blood flows in pathological scenarios.

This work is organized as follows. We first describe in Section 2 our mathematical and numerical model for the simulation of an idealized left heart by considering the presence of the heart valves and a prescribed wall displacement, for which we propose to use the VMS-LES formulation. We use physiological data to set up our problem and obtain realistic results. In Section 3 we report the numerical results and analyze the outputs in an extensive manner in terms of instantaneous and phase averaged fields, as well as other meaningful fluid dynamics indicators; a comparison of the results obtained by means of the VMS-LES formulation and SUPG stabilization is also performed. We also provide and discuss in Section 3 the numerical results corresponding to the mitral valve regurgitation. Finally, we draw our conclusions in Section 4, wherein we also discuss the limitations of our approach and possible future developments.

## 2 | THE MATHEMATICAL AND NUMERICAL MODEL

Several aspects need to be taken into consideration for a realistic simulation of the fluid dynamics in the left heart. First, the blood is composed of a liquid phase, the plasma, and of solid cells and platelets carried by the flow, therefore its rheology is namely rather complex [8,22,41]. However, in large vessels, as well as in the heart chambers, it can be assumed that the blood behaves like a Newtonian fluid with constant properties (density and viscosity). Hence, in the following, we consider the blood to be an incompressible Newtonian fluid with density $\rho = 1.06$ g/cm$^3$ and dynamic viscosity $\mu = 0.035$ g/(cm s). These properties are typical of a very viscous fluid; therefore, in small arteries and veins, the flow regime is usually laminar. On the other hand, in the left heart chambers we find the largest flow velocities in the whole cardiovascular system, specifically across the valve sections, where the Reynolds number can become as large as 5000 [22]. In these conditions, the flow can become transitional or nearly turbulent and a reliable turbulence model should be considered in combination with the incompressible Navier-Stokes equations if Direct Numerical Simulations cannot be performed.

The left heart can be regarded as a pump that collects the oxygenated blood from the lungs and pushes it into the systemic circulation through the aorta. This is made possible by the concerted action of electromechanics phenomena, that is the propagation of an electric signal through the myocardium which triggers mechanical contraction and then relaxation of the cardiac muscle. This results in a cyclic deformation of the heart chambers and volume changes along the heartbeat. The left ventricle change in volume is of the order of 70% with respect to its maximum volume while that of the left atrium is about 40%. To account for these large variations in the computational domain of the fluid problem, we use an Arbitrary Lagrangian Eulerian (ALE) reference frame. Another important issue is the manner in which valves are accounted for. The more detailed approach consists in using a fluid-structure interaction (FSI) model in an ALE framework [13,15]: in this case, the valves are considered as three-dimensional structures undergoing mechanical deformation and the fluid-solid interface is represented by their lateral surface. Another approach, which is aimed at accounting for the effect of the valves' leaflets on the fluid, makes use of immersed methods by keeping a single computational domain (the fluid one) and modeling the presence of the valves by means of a resistive method [12,47]. Other reduced approaches consist in mimicking the valves through surrogate models [9] or as mixed time-varying boundary conditions [19].

In this section we discuss all of the mathematical aspects related to the construction of the left heart fluid model. Specifically, we consider the incompressible Navier-Stokes equations in ALE formulation, stabilization methods (VMS and SUPG) and turbulence LES modeling, the left heart chambers and their deformation along the heartbeat, the use of the resistive method to account for the presence of the valves, and finally the boundary conditions at the pulmonary veins and aorta.

## 2.1 | Navier-Stokes equations in ALE framework

The Navier-Stokes equations in a moving domain $\Omega_t$ that depends on the time $t$ can be written as:

$$\nabla \cdot \mathbf{v} = 0 \qquad \text{in } \Omega_t, \quad t > 0\,, \tag{1}$$

$$\rho \frac{\hat{\partial}\mathbf{v}}{\partial t} + \rho\left(\mathbf{v} - \mathbf{v}_{ALE}\right) \cdot \nabla \mathbf{v} = \nabla \cdot \mathbf{T}(\mathbf{v}, p) \qquad \text{in } \Omega_t, \quad t > 0\,, \tag{2}$$

endowed with suitable boundary and initial conditions. In (1)-(2) $\rho$ is the fluid density, $\frac{\hat{\partial}}{\partial t}$ represents the time derivative in the ALE framework, $\mathbf{v}_{ALE}$ is the domain velocity and the Cauchy stress tensor $\mathbf{T}(\mathbf{v}, p)$ can be written as a function of the fluid pressure $p$ and velocity field $\mathbf{v}$ through the strain rate tensor $\mathbf{S}(\mathbf{v})$ as:

$$\mathbf{T}(\mathbf{v}, p) = -p\mathbf{I} + 2\,\mu\,\mathbf{S}(\mathbf{v})\,, \tag{3}$$

$$\mathbf{S}(\mathbf{v}) = \frac{1}{2}\left(\nabla \mathbf{v} + \nabla \mathbf{v}^T\right)\,, \tag{4}$$

where $\mu$ is the dynamic viscosity . We also define the advective velocity $\mathbf{v}_a = \mathbf{v} - \mathbf{v}_{ALE}$. The domain velocity $\mathbf{v}_{ALE}$ is determined by prescribing, for each $t > 0$, its value on the boundary $\Gamma_t$ of $\Omega_t$ which is then extended in the computational domain through the following harmonic extension[42]:

$$\begin{aligned} -\nabla \cdot \left(\mathbf{K}\,\nabla \mathbf{v}_{ALE}\right) &= \mathbf{0} && \text{in } \Omega_t\,, \\ \mathbf{v}_{ALE} &= \mathbf{v}_{dALE} && \text{on } \Gamma_t\,; \end{aligned} \tag{5}$$

$\mathbf{K}$ is a tensor to be properly set to ensure preservation of the geometric properties of the domain and later the mesh upon the introduction of the Finite Element discretization[42].

Now, we introduce the infinite dimensional functional spaces needed to write the variational or weak formulation of problem (1)-(2). Let us assume that the boundary $\Gamma_t$ of $\Omega_t$ can be split in $\Gamma_{d,t}$, where a Dirichlet boundary condition is applied, and $\Gamma_{n,t}$, where a homogeneous Neumann condition is instead applied, such that $\Gamma_t = \Gamma_{d,t} \cup \Gamma_{n,t}$. Then, we define the space of integrable functions in $\Omega_t$ as $Q = L^2(\Omega_t)$ and the spaces of weakly differentiable functions $\mathcal{V}_{d,t} = \{\mathbf{u} \in H^1(\Omega_t) \,:\, \mathbf{u} = \mathbf{v}_d \text{ on } \Gamma_{d,t}\}$, where $\mathbf{v}_d$ is the Dirichlet data on the boundary, and $\mathcal{V}_{0,t} = \{\mathbf{u} \in H^1(\Omega_t) \,:\, \mathbf{u} = \mathbf{0} \text{ on } \Gamma_{d,t}\}$. The weak formulation of Navier-Stokes equations in ALE framework consists in finding, for any $t > 0$, $(\mathbf{v}, p) \in \mathcal{V}_{d,t} \times Q$ such that for all $(\mathbf{w}, q) \in \mathcal{V}_{0,t} \times Q$:

$$\int_{\Omega_t} \nabla \cdot \mathbf{v}\, q\, d\Omega = 0\,, \tag{6}$$

$$\int_{\Omega_t} \left[\left(\rho \frac{\hat{\partial}\mathbf{v}}{\partial t} + \rho(\mathbf{v} - \mathbf{v}_{ALE}) \cdot \nabla \mathbf{v}\right) \cdot \mathbf{w} + \mathbf{T}(\mathbf{v}, p) \,:\, \nabla \mathbf{w}\right] d\Omega = 0\,. \tag{7}$$

In view of the introduction of the Variational Multiscale (VMS) method, we now assume a multiscale decomposition of the spaces $\mathcal{V}_{d,t}$, $\mathcal{V}_{0,t}$ and $Q$ in the form $S = S^h \oplus S'$ with $S^h$ a suitable finite dimensional space and $S'$ an infinite dimensional one. Specifically, the space $S^h$ is built upon the finite element space $\mathcal{X}_h^r = \{\mathbf{v}_h \,:\, \Omega_t \to \mathcal{R} \,:\, \mathbf{v}_h|_k \in \mathcal{P}_r \quad \forall k \in \tau_h\}$, with $r$ the polynomial degree and $\tau_h$ the partition of $\Omega_0$ into mesh elements (tetrahedrons in our case); the rest of the space notation is understood. In this way, every function we have defined on the spaces $\mathcal{V}_{d,t}$, $\mathcal{V}_{0,t}$ and $Q$, can be written (decomposed) as the sum of a coarse scale and a fine scale component,

$$\mathbf{v} = \mathbf{v}^h + \mathbf{v}' \qquad p = p^h + p' \qquad \mathbf{w} = \mathbf{w}^h + \mathbf{w}' \qquad q = q^h + q'\,.$$

By representing (6)-(7) into coarse and fine scale components and integrating by parts the fine scale terms into the coarse scale equations we obtain the coarse scale equations, with the fine scale terms not appearing under differential operators[40,43]. We

close the problem by modeling the fine scales as:

$$\mathbf{v}' = -\tau_M(\mathbf{v}^h)\,\mathbf{r}_m(\mathbf{v}^h, p^h) \tag{8}$$

$$p' = -\tau_C(\mathbf{v}^h)\,r_c(\mathbf{v}^h)\,, \tag{9}$$

where $\mathbf{r}_m(\mathbf{v}^h, p^h)$ and $r_c(\mathbf{v}^h)$ are the element-wise strong residuals of (2) and (1), respectively:

$$\mathbf{r}_m(\mathbf{v}^h, p^h) = \rho\frac{\hat{\partial}\mathbf{v}^h}{\partial t} + \rho(\mathbf{v}^h - \mathbf{v}_{ALE})\cdot\nabla\mathbf{v}^h - \nabla\cdot\mathbf{T}(\mathbf{v}^h, p^h)\,, \tag{10}$$

$$r_c(\mathbf{v}^h) = \nabla\cdot\mathbf{v}^h\,. \tag{11}$$

The stabilization parameters $\tau_M(\mathbf{v}^h)$ and $\tau_C(\mathbf{v}^h)$ will be defined later. The coarse scale solution $(\mathbf{v}^h, p^h)$ coincides with the finite element approximation of the incompressible Navier-Stokes equations with a residual-based stabilization technique dependent on Eqs. (8)-(9).

In this work we use a Backward Differentiation Formula (BDF) of order $\sigma$ for the time discretization following the Finite Element approximation of the problem. As BDF formulas yield fully implicit schemes, their use in the nonlinear problem calls for suitable methods for addressing the nonlinearity arising at each time step of the simulations, such as fixed point or Newton methods. A manner to overcome this issue consists in using a semi-implicit formulation for the solution of the incompressible Navier-Stokes equations as proposed in[43]. Specifically, the nonlinear terms are "linearized" by means of a Newton-Gregory extrapolation of order $\sigma$; such extrapolation is based on the solution already computed at the previous time steps[43]. In this way, a linear system needs to be solved at each time step: the method is computationally cheaper than fully implicit methods, but restrictions on the time step size should be accounted for stability reasons. As a matter of fact, in hemodynamics simulations, the choice of the time step size is typically driven by accuracy considerations ($\Delta t < 10^{-3}$ s) for which stability issues with semi-implicit formulations are rarely encountered.

In this paper, we use the semi-implicit BDF method for the time discretization of the Navier-Stokes equations with VMS-LES modeling of[43], which we recast in ALE formulation to account for the deformation of the computational domain $\Omega_t$.

## 2.2 | Left heart geometry and wall displacement

The left heart (LH) is composed of two chambers, the left atrium (LA) and the left ventricle (LV), which are separated by the mitral valve. Four pulmonary veins (PV) are connected to the left atrium (LA) to feed the LA with oxygenated blood from the lungs; similarly, the LV is connected to the aorta through the aortic valve (AV). We consider the LH geometry as an idealized LA (see[44,45]) anchored to an idealized LV represented by half of a prolate ellipsoid, see e.g.[18,19,20]. In this work, we match the base of the LA with the LV through an idealized mitral valve section which is about 5 cm$^2$ wide. Moreover, we model the aortic root as a cylinder whose diameter is $D_{AV} = 3$ cm and the pulmonary veins as four equally sized cylinders with diameter $D_{PV} = 1.5$ cm. The geometry of the idealized LH at the end systolic phase (for the LV), i.e. when the LV volume is smaller than the LA one, is reported in Figure 1. Here we limit to consider the volume occupied by the blood, for which there are time windows along the heartbeat in which the LV volume is actually smaller than the LA one. In the time instant reported in Figure 1, corresponding to $t = 0$ s in Figure 3, the LV volume is approximately 53 mL, while the LA volume is 92 mL. The left atrial appendage (LAA) is a small chamber connected to the atrium through an orifice. LAA and its orifice show a morphology significantly variable across the population individuals for which four recurrent configurations have been classified[46]. The one reported in Figure 1 basically corresponds to a "CauliFlower" type LAA; see[21,46].

The physiological heart cycle is divided into two main phases, the diastole and the systole, which are typically referred to the LV (indeed, while each chamber has its own diastolic and systolic phases, heart phases are conventionally coincident with those of the LV). We define $T_{hb}$ the total time length (duration) of one heartbeat, $t_{dias}$ the duration of the diastole and $t_{syst}$ of the systole. During diastole, blood enters in the LA from the pulmonary veins and flows to the LV passing through the MV, which is open. The AV is closed so that the blood cannot flow out of the LV. The LV expands during this phase while the LA reduces its size with a complex dynamics. The volume reduction of the LA is due to the LV movement towards the LA and to atrial contraction occurring in the last part of the diastole. When the LV stops its expansion and starts contracting, the MV closes due to the pressure difference across the chambers; a rapid iso-volumetric phase takes place in which the LV pressure rises until it overtakes the aortic pressure, so that the AV opens. The systole is the phase during which the LV contracts, the oxygenated blood is pushed from the LV into the aorta, the LA dilates and is filled with blood coming from the PVs. In this phase, the MV is closed. Finally, after the LV has attained its minimum volume, it starts expanding again, the intraventricular pressure drops and the AV closes due to the pressure difference between the aorta and the LV. There is another rapid iso-volumetric phase in

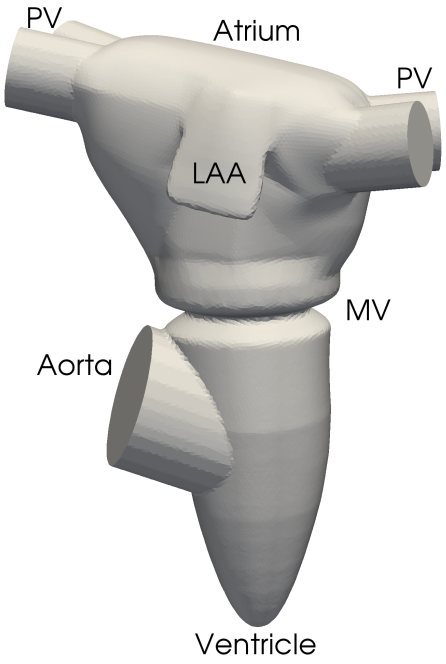


**FIGURE 1** The idealized LH geometry at the end systolic phase for the LV. The left atrium (LA) is located on top of the left ventricle (LV); the two chambers are separated by the mitral valve section (MV). The aortic root is attached to the LV. The pulmonary veins (PV) and the left atrial appendage (LAA) are also indicated

which both of the valves are closed and the LV pressure drops until it reaches the LA values; subsequently the MV opens and a new heart cycle begins. These phases are represented in the well known Wiggers diagram[8,29]. From a modeling point of view, since we assume the blood to be an incompressible fluid, we cannot straightforwardly represent the iso-volumetric phases when the pressure change is due to small volume variations. With this aim, one should allow some limited compressibility to the fluid so that this process can be captured. However, since these phases are very rapid, we assume the switch between diastole and systole to be instantaneous as well as valves change in configuration from open to closed and viceversa. Therefore, there are only two possible configurations in our fluid dynamics model for the LH: i) diastole with LV expanding, LA contracting, MV open and AV closed; ii) systole with LV contracting, LA expanding, MV closed and AV open.

In order to model the wall displacement of the LH chambers (LA and LV), we assume the variations in volume to be in the physiological range, with the LV volume in the range of 53 to 164 mL, while LA volumes spans in the 55 to 92 mL range[3]. In order to setup the LA and LV wall displacement and deformation, we assume several other constraints. Among these, the ratio between the height and the diameter of the LV is kept around $1.7 \div 2$ [18,22,32]. Moreover, the LV apex movement is directed towards the LA. Finally, we assume that the LA volume variation is similar to the one of a sphere with changing volume, so that the displacement is directed towards the center of the LA. With these constraints, we proceed by separating time and space independent variables in the definition of the wall displacement of the heart chambers $\mathbf{v}_{dALE}$ as done in[45]. The volume variation in time should correctly represent two different filling stages of the LV during diastole, called the Early wave (E-wave) and the After wave (A-wave). We report in Figure 2 the volume against time for the idealized LV and LA. These are obtained with a Fourier expansion in time of the volume reported in[18] that we adapted to the LA geometry.

The wall displacements of the LA and LV are prescribed similarly to the approach used in[45] for the LA alone. The wall displacement velocity of the left heart $\mathbf{v}_{dALE}$ is selected as:

$$\mathbf{v}_{dALE}(\mathbf{x}, t) = \mathbf{f}_{ven}(\mathbf{x}) \frac{dr_{ven}}{dt}(t) + \mathbf{f}_{atr}(\mathbf{x}) \frac{dr_{atr}}{dt}(t),$$

where the vector valued functions $\mathbf{f}_{ven}(\mathbf{x})$ and $\mathbf{f}_{atr}(\mathbf{x})$ assimilate the displacements of the LV and LA walls to those of spheres and are chosen to represent realistic deformations of the whole left heart; $\frac{dr_{ven}}{dt}(t)$ and $\frac{dr_{atr}}{dt}(t)$ account instead for the evolution in time of the LV and LA volumes, say $V_{ven}(t)$ and $V_{atr}(t)$, respectively. In particular, following[45], we set

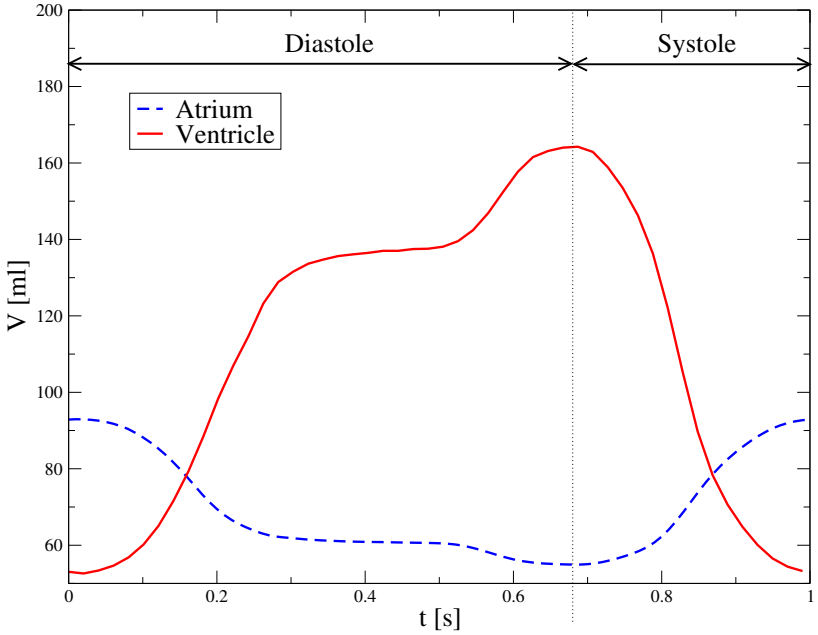


**FIGURE 2** Volumes of the left atrium (LA) and left ventricle (LV) vs. time along the heartbeat

$\frac{dr_{ven}}{dt}(t) = \frac{V_{ven}(t)^{-2/3}}{3}\frac{dV_{ven}}{dt}(t)$ and $\frac{dr_{atr}}{dt}(t) = \frac{V_{atr}(t)^{-2/3}}{3}\frac{dV_{atr}}{dt}(t)$, where $V_{ven}(t)$ and $V_{atr}(t)$ are those displayed in Figure 2. Twisting effects of the left ventricle wall are however neglected in the current idealized model. Even if our choice does not ensure a perfect match of the LV and LA volume changes over time with the Wiggers diagram, our approximation allows obtaining in a simple and accurate fashion physiological wall displacements of the chambers.

In Figure 3 we display snapshots of the geometry of the LH at several time instants along the heartbeat. Being based on an analytical characterization of the wall displacement, our model can be easily parametrized in order to represent a wide range of physiological variability among patients.

## 2.3 | Heart valves

Modeling the heart valves is a challenging problem that has widely been investigated and is still currently being extensively studied, see e.g. [12,13,15,16,17,26,47]. The dynamics of the leaflets is very complex and subject to strong fluid-structure interaction. In some preliminary studies [26], the valve dynamics is approximated by a zero-dimensional model, according to which the state of the valve is completely determined by a few variables, such as the leaflets angle or the valve orifice area. Usually, these models take into account for the pressure drop across the valve orifice, the blood flux through the valve and few other variables, yielding a system of Ordinary Differential Equations (ODEs) [12,26]. In other works [13,16,17,47], the valve is instead considered as a three-dimensional domain and a full fluid-structure interaction problem is solved, either in a moving mesh framework or with immersed methods. In this work instead, we assume that the valve dynamics is known *a priori* according to the phase of the heartbeat determined by the Wiggers diagram; we consider the interactions of the valve with the fluid to be limited to a no-slip condition at the valve leaflets or, better saying, that the fluid adheres to the valve when it is closed. Similarly to [19,20], we model only the fluid problem in a deforming domain and we account for the effect of the valves on the blood flow dynamics. To achieve this goal we use a resistive method as in [12], and we assume the valves to be in either their open or closed configurations. We do not explicitly represent the valve leaflets, but rather we let them instantaneously "dissolve" when the valve enters in the open configuration; when the valve closes instead, a barrier suddenly materialize ideally to disconnect chambers in the LH. In this latter case, we identify the regions (AV for aortic valve and MV for mitral valve) occupied by the valves in their closed configurations in which we set the fluid velocity $\mathbf{v}$ to be equal to the domain velocity $\mathbf{v}_{ALE}$. In Figure 4, we report the location where we enforce the fluid velocity to be equal to the domain velocity for closed valves. We remark that AV is closed during diastole, while the MV is closed during systole. Pressure changes in the heart chambers and jumps across valves are naturally accomplished by means of the resistive method; see [12].

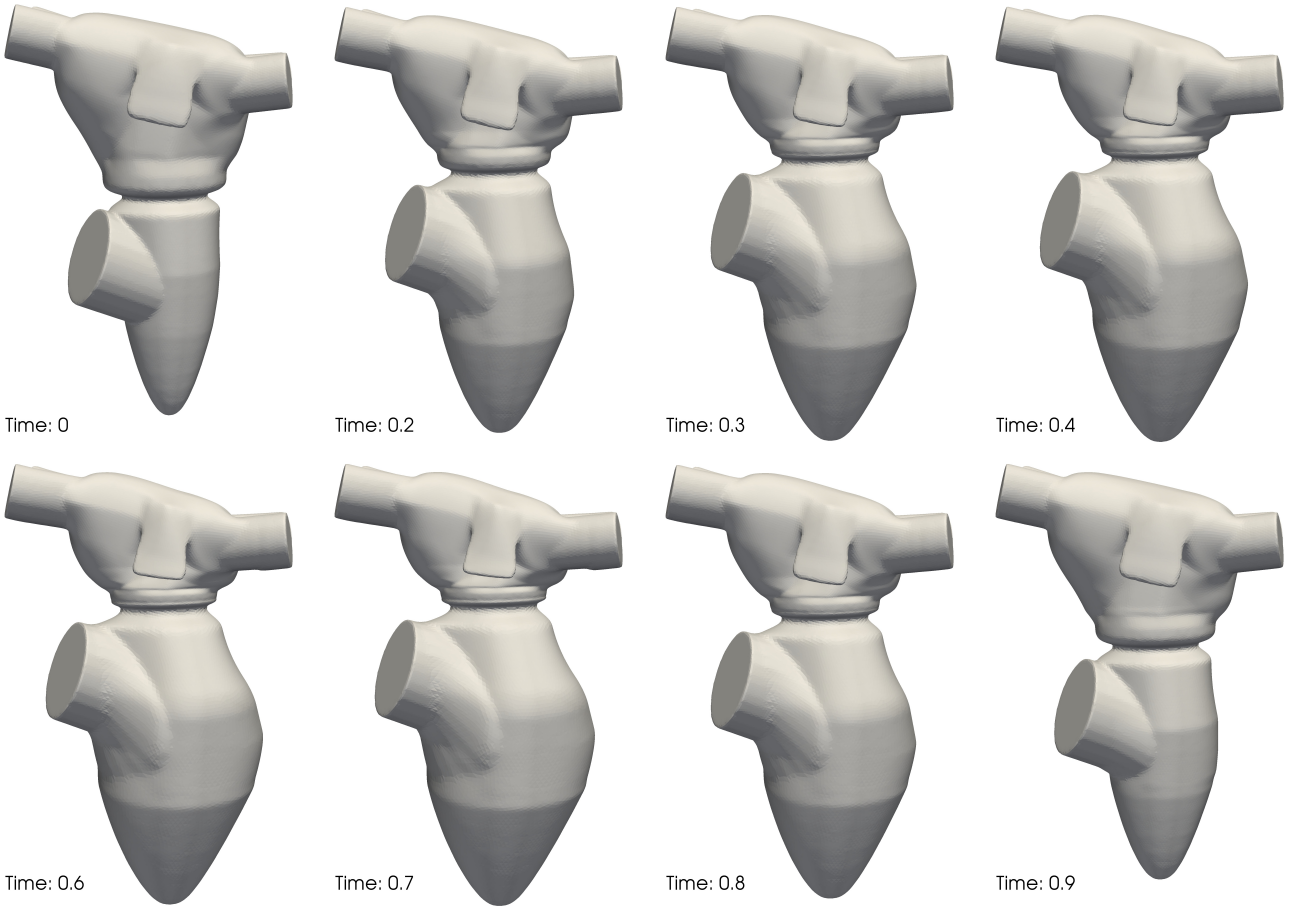


**FIGURE 3** Configuration of the LH geometry at different time instants of the heartbeat

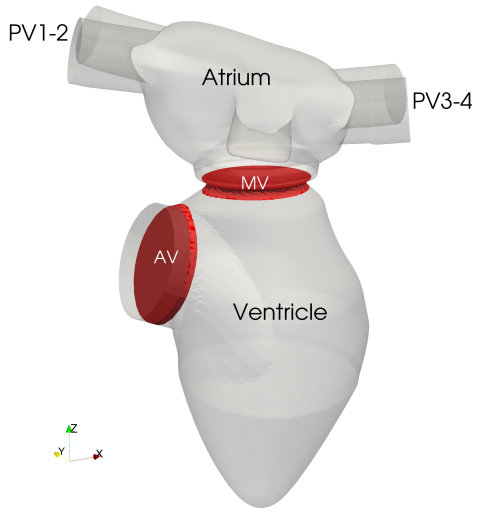


**FIGURE 4** Locations of the mitral (MV) and aortic (AV) valves in the LH geometry. The subsets of the LH in red stands for the region in the domain where the velocity is enforced to adhere to the domain velocity when the valves are closed, i.e. during diastole for the aortic valve and during systole for the mitral valve

In order to account for the valves with the resistive method [12], the momentum equation in weak formulation (7) is supplemented with an additional term, say

$$\int_{\Omega_t} R_h \left(\mathbf{v} - \mathbf{v}_{ALE}\right) \cdot \mathbf{w}\, d\Omega\,; \tag{12}$$

the function $R_h$ has support in thin subsets of $\Omega_t$ wherein the valves leaflets lay. $R_h$ plays the role of a smoothed Dirac function across the valve leaflet; albeit its support is limited to a region of thickness corresponding to few mesh elements (typically $2h$ wide with $h$ the mesh size), the value of $\|R_h\|_{L^2}(\Omega_t)$ is "sufficiently" large to effectively and locally enforce the adherence of the fluid velocity to the domain deformation velocity $\mathbf{v}_{ALE}$. We notice that $R_h = R_h(\mathbf{x}, t)$ as the valve leaflets move over the time [12]. In this work, following the Finite Element discretization, we use a function $R_h$ which is piecewise discontinuous onto the Finite Element mesh by mimicking the behavior of a 1D function $\widetilde{\delta}_h(x)$ such that $\widetilde{\delta}_h(x) = 0$ for $|x| > h$ and $\widetilde{\delta}_h(x) = R/h$ for $|x| \leq h$, with $R \in \mathbb{R}^+$.

We modify the VMS-LES formulation of the Navier-Stokes equations in the ALE framework to account for the presence of the resistive term. The definition of the stabilization parameters [12,40,43] becomes now:

$$\tau_M(\mathbf{v}^h) = \left(\frac{\rho^2\sigma^2}{\Delta t^2} + \rho^2\, \mathbf{v}_a^h \cdot \mathcal{G}\, \mathbf{v}_a^h + \overline{C}\mu^2\, \mathcal{G} : \mathcal{G} + R^2\right)^{-\frac{1}{2}}, \tag{13}$$

$$\tau_C(\mathbf{v}^h) = \frac{1}{\tau_M(\mathbf{v}^h)\mathbf{g} \cdot \mathbf{g}}, \tag{14}$$

where $\sigma$ is a constant equal to the order of the BDF formula, $\overline{C} = 60$, $\mathcal{G}$ is a second-rank metric tensor and $\mathbf{g}$ is the metric vector:

$$\mathcal{G} = \left(\frac{\partial \boldsymbol{\xi}}{\partial \mathbf{x}}\right)^T \frac{\partial \boldsymbol{\xi}}{\partial \mathbf{x}}, \tag{15}$$

$$\mathbf{g} = \sum_{j=1}^{3} \left(\frac{\partial \boldsymbol{\xi}}{\partial \mathbf{x}}\right)_{ji}, \tag{16}$$

where $\frac{\partial \boldsymbol{\xi}}{\partial \mathbf{x}}$ is the inverse Jacobian of the mapping between the reference and the physical domain. See [40,43] for more details.

To summarize, the VMS-LES formulation for the Navier-Stokes equations in the ALE framework and with resistive term is: find, for each time $t > 0$, $(\mathbf{v}^h, p^h) \in \mathcal{V}_{d,t}^h \times Q^h$ such that, for all $(\mathbf{w}^h, q^h) \in \mathcal{V}_{0,t}^h \times Q^h$

$$\int_{\Omega_t} \left(\nabla \cdot \mathbf{v}^h\, q^h - \mathbf{v}' \cdot \nabla q^h\right) d\Omega = 0\,, \tag{17}$$

$$\begin{aligned}
&\int_{\Omega_t} \left[\left(\frac{\hat{\partial}\mathbf{v}^h}{\partial t} + \rho(\mathbf{v}_h - \mathbf{v}_{ALE}) \cdot \nabla \mathbf{v}^h + R\left(\mathbf{v}^h - \mathbf{v}_{ALE}\right)\right) \cdot \mathbf{w}^h + \mathbf{T}^h : \nabla \mathbf{w}^h\right] d\Omega \\
&- \int_{\Omega_t} \left[\mathbf{v}' \cdot (\rho(\mathbf{v}_h - \mathbf{v}_{ALE}) \cdot \nabla \mathbf{w}^h) - p' \nabla \cdot \mathbf{w}^h\right] d\Omega \\
&- \int_{\Omega_t} \mathbf{v}' \cdot (\rho(\mathbf{v}_h - \mathbf{v}_{ALE}) \cdot (\nabla \mathbf{w}^h)^T)\, d\Omega \\
&- \int_{\Omega_t} (\mathbf{v}' \otimes \mathbf{v}') \cdot \nabla \mathbf{w}^h\, d\Omega = 0\,,
\end{aligned} \tag{18}$$

together with initial conditions $\mathbf{v} = \mathbf{0}$ and the fine scale velocity and pressure $\mathbf{v}'$, $p'$ defined as in (8)-(9). The definition of the residual $\mathbf{r}_m(\mathbf{v}^h, p^h)$ in (8) is modified, to account for (12),

$$\mathbf{r}_m(\mathbf{v}^h, p^h) = \rho \frac{\hat{\partial}\mathbf{v}^h}{\partial t} + \rho(\mathbf{v}^h - \mathbf{v}_{ALE}) \cdot \nabla \mathbf{v}^h + R_h\left(\mathbf{v}^h - \mathbf{v}_{ALE}\right) - \nabla \cdot \mathbf{T}(\mathbf{v}^h, p^h)\,. \tag{19}$$

We remark that in (18) the first term is the residual of the momentum equation, the second term accounts for the standard SUPG stabilization method of the Navier-Stokes equations, the third term stems from the VMS modeling and the fourth term corresponds to the Reynolds stress term, which yields the VMS-LES modeling using (8). Therefore, SUPG stabilization of the Navier-Stokes equations in the ALE framework with resistive method is obtained simply by removing the last two terms in (18).

## 2.4 | Boundary conditions

Based on the Wiggers diagram, the boundary conditions differ when considering diastole and systole since the valve behavior has a strong influence on the flow. In particular, during diastole, the AV is closed and the whole volume variation of the LH must be balanced by an equal blood inflow from the PVs. During systole, the flow rate in the LA coming from the PVs must be equal to the LA volume variation, while the aorta outflow is equal to the LV volume variation. Since the flow is periodic, we define the boundary conditions on a time period corresponding to a single heartbeat time $T_{hb}$, and then, for every new heartbeat, the same boundary conditions are applied. By defining $t^* \in [0, T_{hb})$ as the time instance in the reference heartbeat we have the blood flow rate $Q_{PV}$ at the PVs:

$$Q_{PV} = \begin{cases} \dfrac{dV_{ven}}{dt} + \dfrac{dV_{atr}}{dt} & t^* \in [0, t_{dias}]\,. \\ \dfrac{dV_{atr}}{dt} & t^* \in (t_{dias}, T_{hb})\,. \end{cases} \tag{20}$$

We assume the inflow at the PVs to be equally split among the veins and a parabolic velocity profile: indeed, blood flow in the PVs can be assumed to be laminar. To define a parabolic profile in each vein, we solve an additional problem for a scalar variable $\chi$ in the volume $\Omega_t$, see Figure 1, written as:

$$\begin{aligned} -\Delta\chi &= 1 && \text{in} \quad \Omega_t\,, \\ \chi &= 0 && \text{on} \quad \Gamma_{w,t}\,, \\ \nabla\chi \cdot \mathbf{n} &= 0 && \text{on} \quad \Gamma_{PV,t}\,, \end{aligned} \tag{21}$$

where $\Gamma_{PV,t}$ is the inlet surface of the pulmonary veins and $\Gamma_{w,t} = \Gamma_t \backslash \Gamma_{PV,t}$. The auxiliary variable $\chi$ is used to define a reference inflow velocity profile $\mathbf{v}^i_{ref}$ with total flux equal to 1 on each $i$-th inlet PV as:

$$\mathbf{v}^i_{ref} = \frac{\chi \mathbf{n}}{\int_{\Gamma^i_{PV}} \chi d\Gamma} \qquad i = 1, 2, 3\,,$$

where $\mathbf{n}$ is the unit vector normal to $\Gamma^i_{PV,t}$ and $\Gamma^i_{PV}$ is the subset of $\Gamma_{PV,t}$ to a single pulmonary vein $i = 1, 2, 3$. Given an inflow flux $Q_{PV}$, we rescale the velocity $\mathbf{v}^i_{ref}$ to obtain the Dirichlet boundary condition at the pulmonary vein simply as $\mathbf{v}|_{\Gamma^i_{PV}} = 0.25\, Q_{PV}\, \mathbf{v}^i_{ref}$. On the last pulmonary vein, $i = 4$, we set a Neumann boundary condition in order to determine the blood pressure in the LA during the whole heart cycle. Based on physiological data, we choose the pressure at the $4^{th}$ pulmonary vein to be constant over time and equal to 10 mmHg.

The boundary conditions at the outlet of the left heart, namely at the aorta section behind the aortic valve, should take into account the rest of the cardiovascular system (systemic circulation) as well as its resistance to the blood flow exiting from the heart. A common way to accommodate this task is to use boundary conditions of resistance type[48,49,50]. The stress at the outlet section is split in its normal and tangential components. Then, the tangential components are set to zero, whereas the normal component is expressed as the sum of two terms, one assigning the minimum pressure of the system and the second one accounting for a resistance due to the outflow. In summary, after denoting the normal unit vector to the outlet boundary with $\mathbf{n}$ and the tangential vectors with $\mathbf{t}_1$ and $\mathbf{t}_2$, we set:

$$\mathbf{T}\,\mathbf{n} = -(C_r\, Q_{out} + p_{ao})\mathbf{n}\,, \qquad \mathbf{T}\,\mathbf{t}_1 = \mathbf{0}\,, \qquad \mathbf{T}\,\mathbf{t}_2 = \mathbf{0}\,,$$

where $Q_{out}$ is the blood flux through the aortic section, $Q_{out} = \int_{\Gamma_{ao}} \mathbf{v}\cdot\mathbf{n}\, d\Gamma$, $C_r$ is a constant that has to be set up to obtain a correct physiological pressure during systole, and $p_{ao}$ is the minimum pressure in the aorta. During diastole, we assume $C_r = 0$ and we set the aortic pressure as evolving linearly in time with physiological values extrapolated from the Wiggers diagram. During systole, the resistance of the circulatory system is active, and we set a minimum arterial pressure of 70 mmHg. Therefore:

$$C_r = \begin{cases} 0 & t^* \in [0, t_{dias}]\,, \\ 400 & t^* \in (t_{dias}, T_{hb}]\,, \end{cases}$$

$$p_{ao} = \begin{cases} 70 - 20\dfrac{t^* - t_{dias}}{t_{dias}} & t^* \in [0, t_{dias}]\,, \\ 70 & t^* \in (t_{dias}, T_{hb}]\,, \end{cases}$$

where the units are [dyn s/cm$^5$] for $C_r$ and [mmHg] for the pressure. We remark that at this stage $Q_{out}$ is unknown being dependent on blood flow velocity at the aortic section.

Finally, blood flow velocity at the LH walls $\Gamma_t \setminus \left(\Gamma_{PV,t} \bigcup \Gamma_{ao,t}\right)$ is set as $\mathbf{v} = \mathbf{v}_{dALE}$ for all $t > 0$, where $\mathbf{v}_{dALE}$ is obtained by deforming the LH domain compatibly with the Wiggers diagram; see Sec. 2.2, Figures 2 and 3, and for reference[45].

## 3 | NUMERICAL RESULTS AND DISCUSSION

Our numerical simulations were carried out by means of the computing resources provided by the Swiss National Supercomputing Center (CSCS) in Lugano using up to 20 nodes of Piz Daint Cray XC40 system. We used $P1$-$P1$ tetrahedral linear elements (degree $r = 1$ for the finite element spaces for both the velocity and pressure variables) and a BDF formula of order $\sigma = 2$ for the time discretization and equal order extrapolation for the nonlinear terms, see[43]. Our software implementation was realized in the open-source finite element library LifeV[51]. We solve the problem by considering the VMS-LES formulation reported in (17-18), as well as the SUPG stabilization method for comparison. For both stabilization methods, in order to obtain a fully developed flow, we initiated the simulations with a zero velocity field and we disregarded the first two heartbeats to remove the effect of this unrealistic initial condition. Then, the simulations are continued for at least further four heartbeats, which we use to analyze the numerical results.

We tested several meshes progressively refined and we finally selected the one with $3'343'277$ elements in the LH and $2'170'320$ degrees of freedom; the average size of the mesh element (tetrahedrons) is therefore at least 0.8 mm, i.e. when the LH volume is maximum along the heartbeat. Our choice was made upon checking *a posteriori* the quality of the LES simulation by using the Pope criterion presented in[38]. According to[38], the fraction of the turbulent kinetic energy in the resolved motions is defined as:

$$M_h(\mathbf{x}, t) = \frac{K_r(\mathbf{x}, t)}{K_h(\mathbf{x}, t) + K_r(\mathbf{x}, t)}, \tag{22}$$

where $K_r$ is the kinetic energy of the unresolved scales and $K_h$ is the kinetic energy of the resolved scales:

$$K_h(\mathbf{x}, t) = \frac{\rho}{2}\, \mathbf{v}_h(\mathbf{x}, t) \cdot \mathbf{v}_h(\mathbf{x}, t), \tag{23}$$

which is available through the computed velocity $\mathbf{v}_h$. Therefore, $M_h$ is a measure of how much energy is actually resolved in the numerical simulation; to perform a "good" quality LES we set a maximum value of $M_h^{max} = 0.2$[38] everywhere in the computational domain for every time along the heartbeat. If the value of $M_h$ is larger than $M_h^{max}$, then one would need to refine the computational mesh. The issue with this approach lays in the evaluation of the kinetic energy of the unresolved scales. In our residual based VMS-LES formulation we propose to use (8) to approximate the unresolved scales, that is

$$K_r(\mathbf{x}, t) = \frac{\rho}{2}\, \mathbf{v}'(\mathbf{x}, t) \cdot \mathbf{v}'(\mathbf{x}, t), \tag{24}$$

We therefore compute $M_h$ as follows:

$$M_h(\mathbf{x}, t) = \frac{\mathbf{v}'(\mathbf{x}, t) \cdot \mathbf{v}'(\mathbf{x}, t)}{\mathbf{v}_h(\mathbf{x}, t) \cdot \mathbf{v}_h(\mathbf{x}, t) + \mathbf{v}'(\mathbf{x}, t) \cdot \mathbf{v}'(\mathbf{x}, t)}. \tag{25}$$

We checked the results of the simulations and we found that with the previously mentioned mesh the largest values of $M_h$ are observed in proximity of the valves and the LA and LV walls, but these never exceed the threshold value $M_h^{max}$. Far from the walls and the valves, we have $M_h < 10^{-4}$ for which we assume that the flow is well resolved using this mesh. As a matter of fact, the results obtained with the VMS-LES formulation are very close to those of a DNS simulation.

### 3.1 | Blood flow dynamics in the left heart

We now describe the numerical results obtained by means of the VMS-LES formulation and time step size $\Delta t = 4 \cdot 10^{-4}$ s. The blood flow in the left heart features a very complex pattern; to visualize it, we use the volume rendering of the instantaneous velocity magnitude in Figure 5 and, in Figure 6, the Q-criterion. The latter represents a standard way to visualize coherent vortex structures in the flow[45]. The $Q$ function is

$$Q = 0.5(|\mathbf{A}|_2 - |\mathbf{S}|_2),$$

where $\mathbf{A}$ and $\mathbf{S}$ are, respectively, the skew-symmetric and symmetric part of the velocity gradient. Coherent vortex structures appear in regions of a positive $Q$; in order to visualize them, we plot the iso-contours of $Q$ by selecting a suitable positive value.

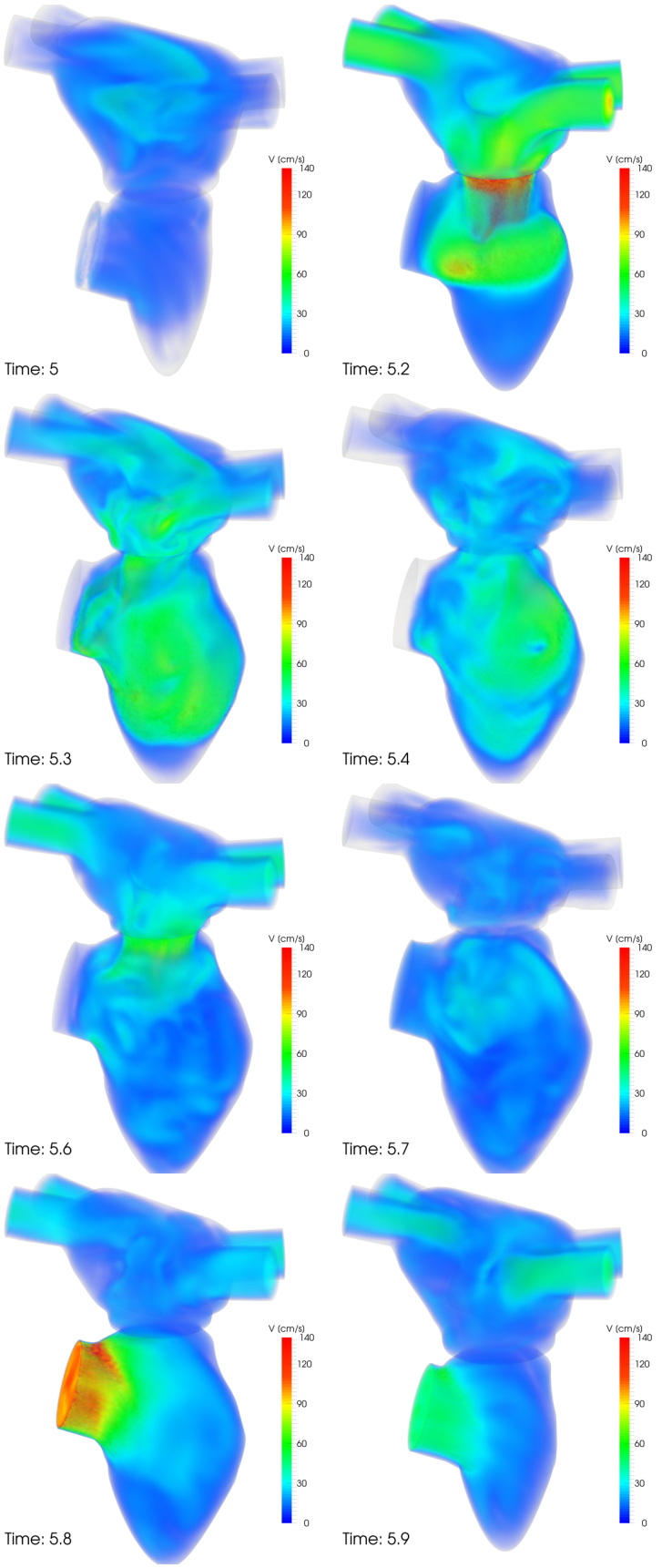


**FIGURE 5** Snapshots of velocity magnitude (volume rendering) at different time instants of the heartbeat

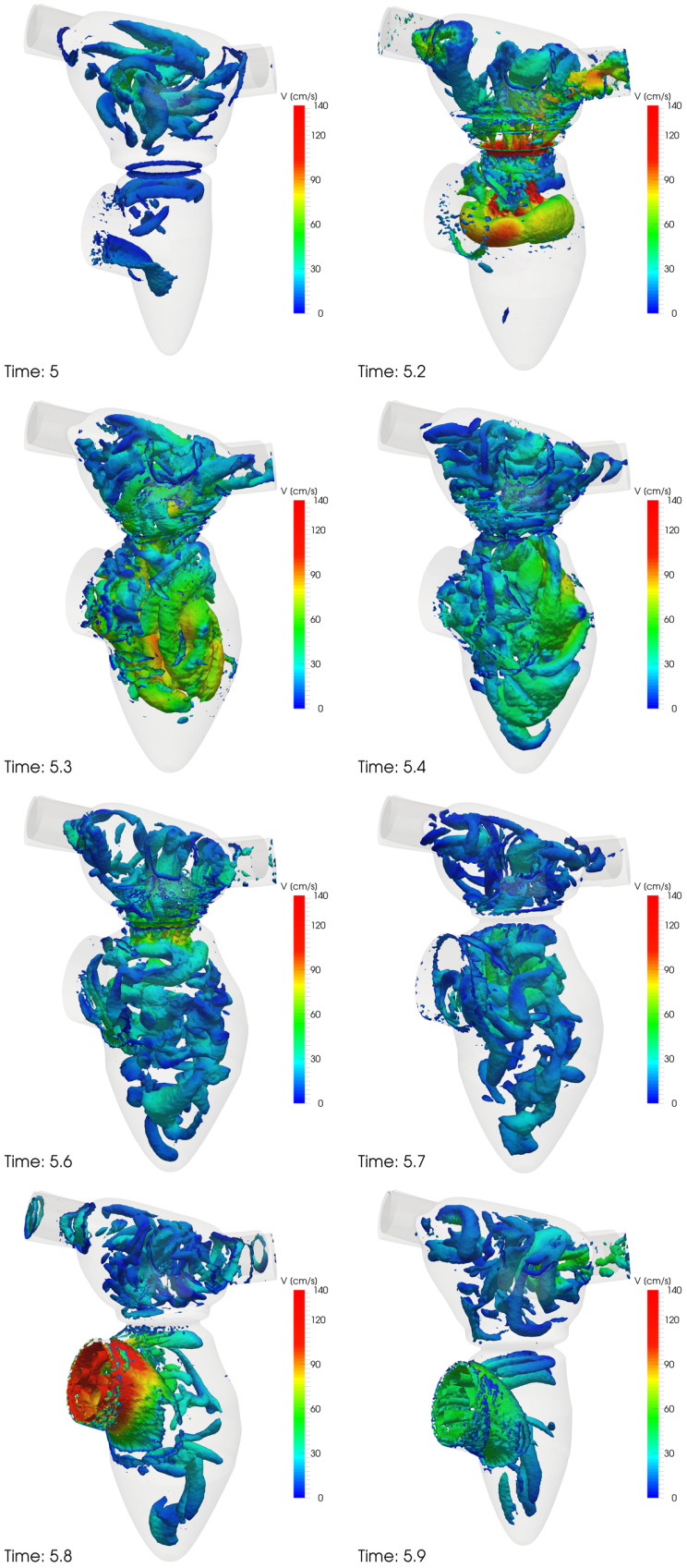


**FIGURE 6** Snapshots of Q-criterion contours (for $Q = 500$) colored by the velocity magnitude at different time instants of the heartbeat

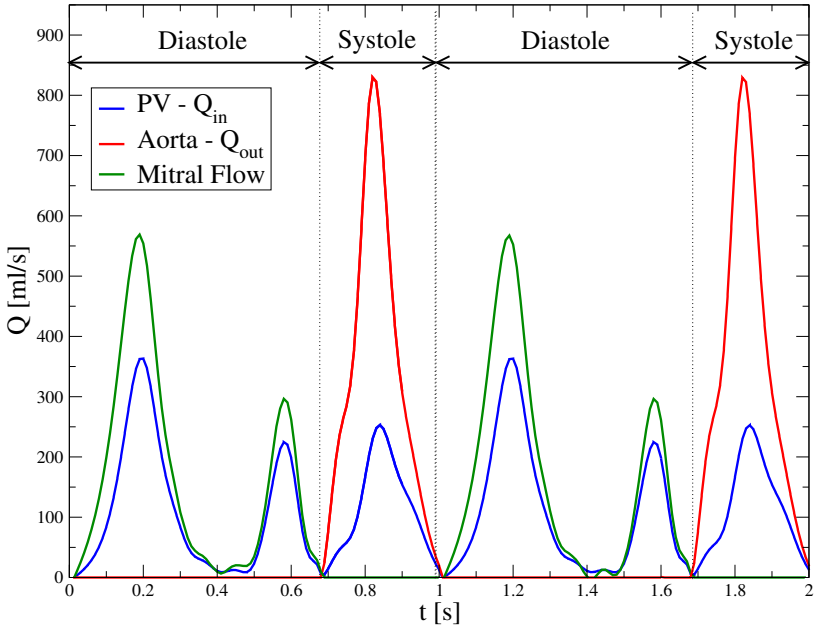


**FIGURE 7** Flow rates through the PVs, the MV section and the aortic section versus time along two heartbeats

In Figure 5, we report the instantaneous velocity magnitude in the left heart at several instants of the sixth heartbeat, when the flow is fully developed. In Figure 6, we display the iso-contours of $Q = 500$ colored according to the velocity magnitude, in the same heartbeat. During early diastole, the velocity is very small, especially in the LV, with some structures still visible in the LA. When the E-wave starts, a high speed flux crosses the MV section and produces a large non-symmetrical structure in the upper part of the LV. The jets coming from the PVs impact in the center of the LA and then progressively dissipate until the A-wave starts. The blood flux through the MV generates a coherent structure in the LV, the so-called O-ring [18,22,36]. The latter breaks into smaller structures as the blood flow moves towards the apex and finally impinges the LV wall. Within the A-wave, a small vortex structure is visible under the mitral section but it is broken immediately at the MV closure and the opening of the AV which marks the beginning of the systole. During systole, a high velocity jet is visible in the aorta and the coherent structures present in the LV are flushed out with the blood flow. The LA is refilled with blood coming from the PVs that produces again an impact between jets, although weaker than the one of the E-wave. At the end of the systole, some structures are still visible in the LA and a small one in the LV just under the mitral section. The velocity is very small apart from the aorta and the veins where inertia is still mixing the blood. All of these features of the blood flow are consistent with those already reported in [18,19,20,22,36].

We post-process the results to obtain the flow rates at the inlet, outlet and mitral sections as reported in Figure 7. The inlet and outlet blood flow rates versus time are reported for the first two heartbeats but, since they correspond to the volume variations, these show negligible differences among heart cycles. The mitral flow, on the other hand, could vary since it depends on the blood flow that develops in the LH; however, we notice that this variable shows the same behavior in time among different heartbeats. A possible explanation is that the mitral flow depends mostly on the wall displacement and volume variations and not on specific features of the flow and geometry. A limitation of this computational study is that the blood flow in the pulmonary veins does not reverse during atrial contraction (A-wave); see Figure 7 for $t \in (0.5, 0.65)$. This is due to the limited variation over time of the LA volume ($\frac{dV_{atr}}{dt}$) during this phase as shown in Figure 2 for $t \in (0.5, 0.65)$ s. Blood flow through the mitral valve in the LV remains however normal in this condition.

In Figure 8, we report the average pressure computed in the LA, in the LV and on the aorta section versus time, for one heartbeat. To evaluate the average pressure in the LA and in the LV, we selected a small volume in approximately the center of each of these chambers and averaged therein the value to obtain the data plotted in Figure 8. In a similar way, we selected a small area in the center of the aorta section and averaged to obtain the pressure at the aorta section. We remark that the pressure in the aorta is prescribed during diastole and that during the first cycle we increase its value starting from zero. During systole, the pressure in the aorta is obtained using the resistance outlet boundary condition [19,48,49,50]. The pressure in the LA shows small oscillations around the average value of 10 mmHg that can be linked to the blood flow coming from the veins. On the other

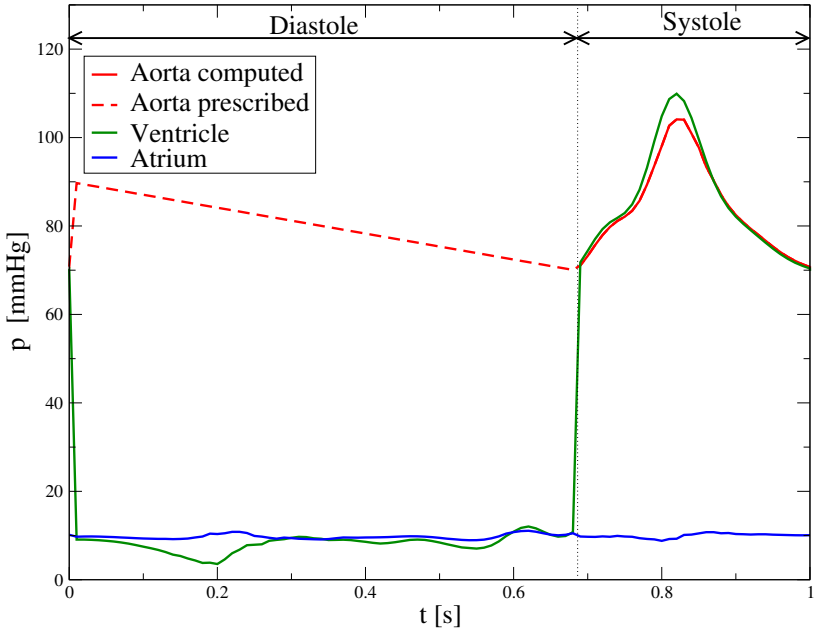


**FIGURE 8** Average blood pressure in the LA, LV and aorta vs. time along one heartbeat

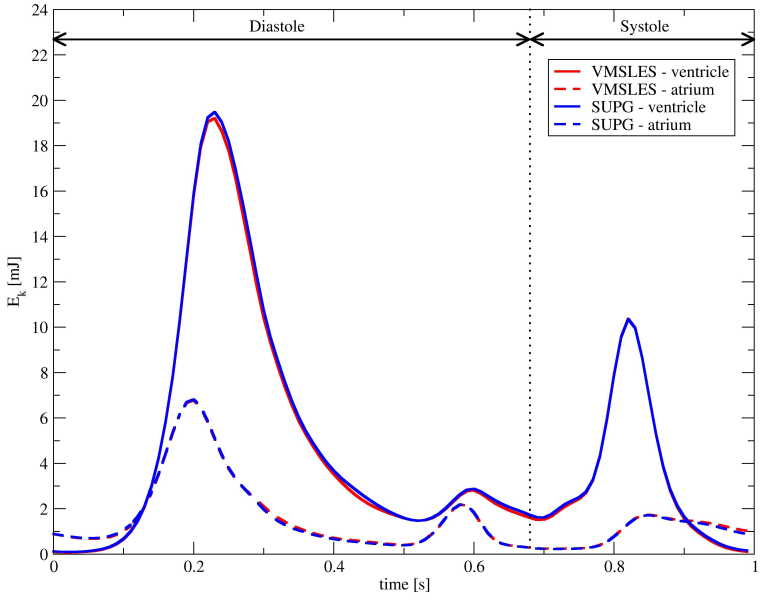


**FIGURE 9** Phase averaged kinetic energy $E_k$ in the LV and LA of the idealized LH vs. time. Results obtained with VMS-LES and SUPG stabilization methods

hand, the pressure in the LV increases when the MV closes and overcomes the pressure in the aorta. In late systole the aortic pressure overcomes the LV pressure and this leads to the closing of the aortic valve with a delay, if a proper valve model is used. In our model the aortic valve simply closes at a fixed time and the LV pressure falls down again to values similar to the LA ones because of the MV opening. The plots of the flow rates and pressure obtained show the same features of the Wiggers diagram.

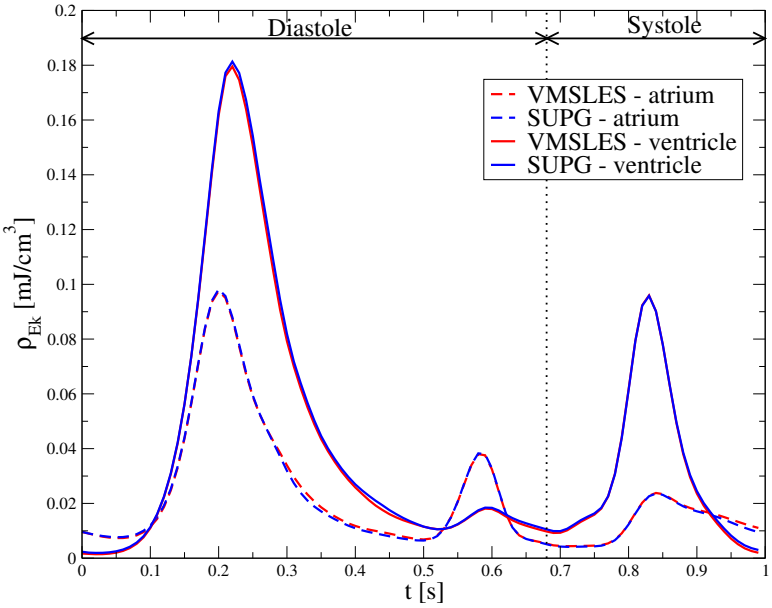


**FIGURE 10** Phase averaged specific kinetic energy $\rho_{Ek}$ in the LV and LA of the idealized LH vs. time. Results obtained with VMS-LES and SUPG stabilization methods

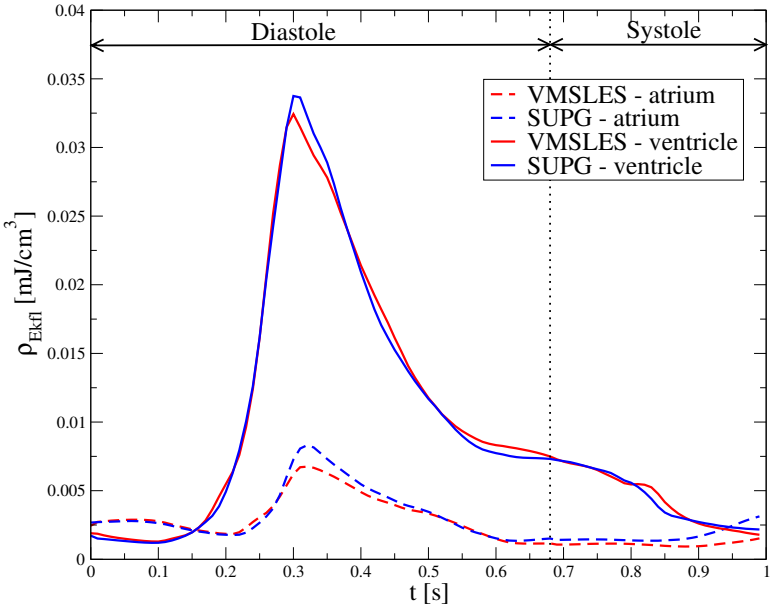


**FIGURE 11** Phase averaged specific fluctuating kinetic energy $\rho_{Ekfl}$ in the LV and LA of the idealized LH vs. time. Results obtained with VMS-LES and SUPG stabilization methods

## 3.2 | Analysis of blood flow dynamics indicators

The heart cycle exhibits periodic features; however, blood flow in the LH is not periodic due to nonlinearity of the model. In order to study and qualify blood flow dynamics along several heartbeats, we perform a phase averaging of the variables. We

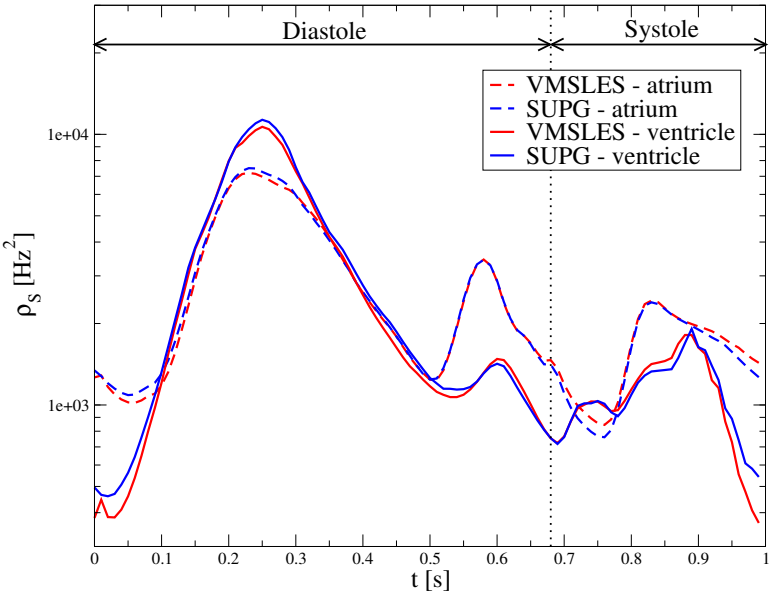


**FIGURE 12** Phase averaged specific enstrophy $\rho_S$ in the LV and LA of the idealized LH vs. time. Results obtained with VMS-LES and SUPG stabilization methods

define the phase average of the velocity field $\overline{\mathbf{v}}$ and its root mean square $\mathbf{v}^{rms}$ as:

$$\overline{v}_i(\mathbf{x}, t^*) = \frac{1}{N_c} \sum_{j=0}^{N_c-1} v_i(\mathbf{x}, t^* + j\, T_{hb}) \qquad t^* \in [0, T_{hb}]\,, \qquad i = 1, 2, 3\,, \tag{26}$$

$$v_i^{rms}(\mathbf{x}, t^*) = \frac{1}{N_c} \sum_{j=0}^{N_c-1} \sqrt{\overline{v_i^2}(\mathbf{x}, t^* + j\, T_{hb}) - \overline{v}_i^2(\mathbf{x}, t^*)} \qquad t^* \in [0, T_{hb}]\,, \quad i = 1, 2, 3\,. \tag{27}$$

We set $N_c = 4$ and we discard the first two heartbeats to remove the influence of the non-physical initial condition $\mathbf{v} = \mathbf{0}$. The quantity $\mathbf{v}^{rms}$ provides information on the flow variability among heartbeats (cycle-to-cycle variations) and can be used as an indicator of transition to turbulence[20]. With these phase averaged quantities we compute some global indicators of the flow, such as the total kinetic energy, the fluctuating kinetic energy and the enstrophy, defined respectively as:

$$E_k(t^*) = \frac{\rho}{2} \int_{\Omega_{t^*}} \overline{\mathbf{v}}(\mathbf{x}, t^*)(\cdot \overline{\mathbf{v}}(\mathbf{x}, t^*)\, d\Omega\,, \tag{28}$$

$$E_{kfl}(t^*) = \frac{\rho}{2} \int_{\Omega_{t^*}} \mathbf{v}^{rms}(\mathbf{x}, t^*) \cdot \mathbf{v}^{rms}(\mathbf{x}, t^*)\, d\Omega\,, \tag{29}$$

$$S(t^*) = \frac{1}{2} \int_{\Omega_{t^*}} \overline{\boldsymbol{\omega}}(\mathbf{x}, t^*) \cdot \overline{\boldsymbol{\omega}}(\mathbf{x}, t^*)\, d\Omega\,, \tag{30}$$

where $\overline{\boldsymbol{\omega}}$ is the vorticity computed with the phase averaged velocity, i.e. $\overline{\boldsymbol{\omega}} = \nabla \times \overline{\mathbf{v}}$. These indicators can provide quantitative information and characterization of the nature of the flow. We report for example in Figure 9 the evolution of the phase averaged total kinetic energy $E_k$ vs. time along heartbeat. The results show that $E_k$ is larger in the LV than in the LA for most of the heartbeat and that it peaks three times for both the LV and LA correspondingly with the E-wave, A-wave, and systolic peak through the aortic valve (mostly the LV only). This and the following numerical results show that the VMS-LES formulation and the standard SUPG stabilization show very similar results, both qualitatively and quantitatively.

In few cases, some of these indicators can be measured experimentally. For example, the total kinetic energy of the blood flow in healthy and diseased left ventricles has been reconstructed by means of Magnetic Resonance Imaging (MRI) 4D flow data[2] to tentatively link it to a physiological or pathological condition of the patient. The values of the total kinetic energy $E_k$ in

| | Diastole | Systole |
|---|---|---|
| LV VMS-LES | 5.06 mJ | 3.35 mJ |
| LV SUPG | 5.19 mJ | 3.40 mJ |
| LV MRI 4D[2] | $2.0 \pm 0.8$ mJ | $1.6 \pm 0.6$ mJ |
| LA VMS-LES | 1.80 mJ | 0.95 mJ |
| LA SUPG | 1.79 mJ | 0.94 mJ |

**TABLE 1** Comparison of the average kinetic energy $E_k$ in the LV and LA during diastole and systole obtained by VMS-LES formulation and SUPG stabilization against those measured by MRI 4D flow data[2]

the LV and LA averaged over the diastolic and systolic phases are reported in Table 1. Results obtained by means of the VMS-LES formulation and SUPG stabilization are quantitatively very similar, and qualitatively inline with the experimental ones. However, the numerical results overestimate by a factor 2 those obtained by the MRI 4D flow data analysis. We believe that this is justified by several technical aspects and limitations connected to MRI 4D flow data measurements like those in[2]: i) the coarser spatial resolution with respect to that of our numerical simulation (3 mm vs. 0.8 mm, or less); ii) the coarser time resolution ($50-55$ ms vs. 0.1 ms); iii) the encoding velocity used to encompass the largest values (set at 100 cm/s while numerical results exhibit peak velocity values above 140 cm/s); iv) the definition of the LV chambers in which velocity measurements are acquired (aortic root is excluded); v) the use of regularization and filtering techniques for the computation of $E_k$. This comparison also highlights the ability of the numerical simulation to provide accurate and highly detailed information accounting for the smallest spatio-temporal scales of the blood flow in the left heart.

As the volumes of the LV and LA chambers vary along the heartbeat, it is more meaningful to assess specific quantities, that is indicators averaged with respect to the chambers volume over time. We define therefore the specific total kinetic energy, fluctuating kinetic energy, and enstrophy:

$$\rho_{Ek}(t^*) = \frac{E_k(t^*)}{\rho\,|\Omega_{t^*}|}, \qquad \rho_{Ekfl}(t^*) = \frac{E_{kfl}(t^*)}{\rho\,|\Omega_{t^*}|}, \qquad \rho_S(t^*) = \frac{S(t^*)}{\rho\,|\Omega_{t^*}|}, \tag{31}$$

in order to study their evolution along the heartbeat. In Figures 10, 11, and 12 we report the specific kinetic energy, the specific fluctuating kinetic energy and the specific enstrophy versus time for the LA and the LV and compare the results obtained with the VMS-LES formulation and SUPG stabilization: again the two numerical approaches methods provide results which are almost not distinguishable.

The specific kinetic energy $\rho_{Ek}(t^*)$ shows a very large peak corresponding to the E-wave in the LA and, with a small delay, in the LV too. A peak corresponding to the A-wave is visible in the LA, while the kinetic energy of the LV does not change significantly during the A-wave. During systole, there is another peak in the LV when blood flows through the aorta and then the kinetic energy shows the minimum value in the heartbeat. In the LA, the refilling leads to a smoother increment of kinetic energy; we also remark that the minimum value of $\rho_{Ek}(t^*)$ in the LA is larger than the one in the LV.

The fluctuating kinetic energy reported in Figure 11 shows a peculiar trend with only one large peak after the E-wave in both the LA and LV. These peaks are delayed with respect to those of the kinetic energy and they correspond to the breakup of the large vortex structures created during the E-wave. This means that the breakup process is highly variable among heartbeats. Moreover, this indicates that transition to turbulence may occur shortly after the diastolic E-wave peak in both the LV and LA chambers, with more evident effects in the LV. The fact that fully developed turbulence is not highlighted in the LH chambers in physiological conditions partially explains the coherence of the results obtained by means of SUPG stabilization and the VMS-LES formulation; we can basically infer that the use of turbulence LES models for this kind of flows in physiological conditions is not strictly necessary, provided that spatial resolution is sufficiently adequate. We also remark that the evolution of $\rho_{Ekfl}(t^*)$ in the LA is flatter than in the LV; this means that the LA flow is more regular across multiple heartbeats.

Finally, we analyze the specific enstrophy $\rho_S(t^*)$. This quantity is strongly linked to the dissipation of the kinetic energy of the flow and it is an indicator of large or small vorticity and, possibly, of transition to turbulence[52,53]. In Figure 12, we report the specific enstrophy vs. time. We again notice the presence of a peak corresponding to the E-wave with some delay in both the LA and the LV and a second peak in the LA. The peaks correspond to the time instants when the kinetic energy is mostly dissipated. Moreover, we remark that the values in the LA and the LV are quite similar, for which we can deduce that the blood flow in the two chambers shows similar vorticity and dissipative features.

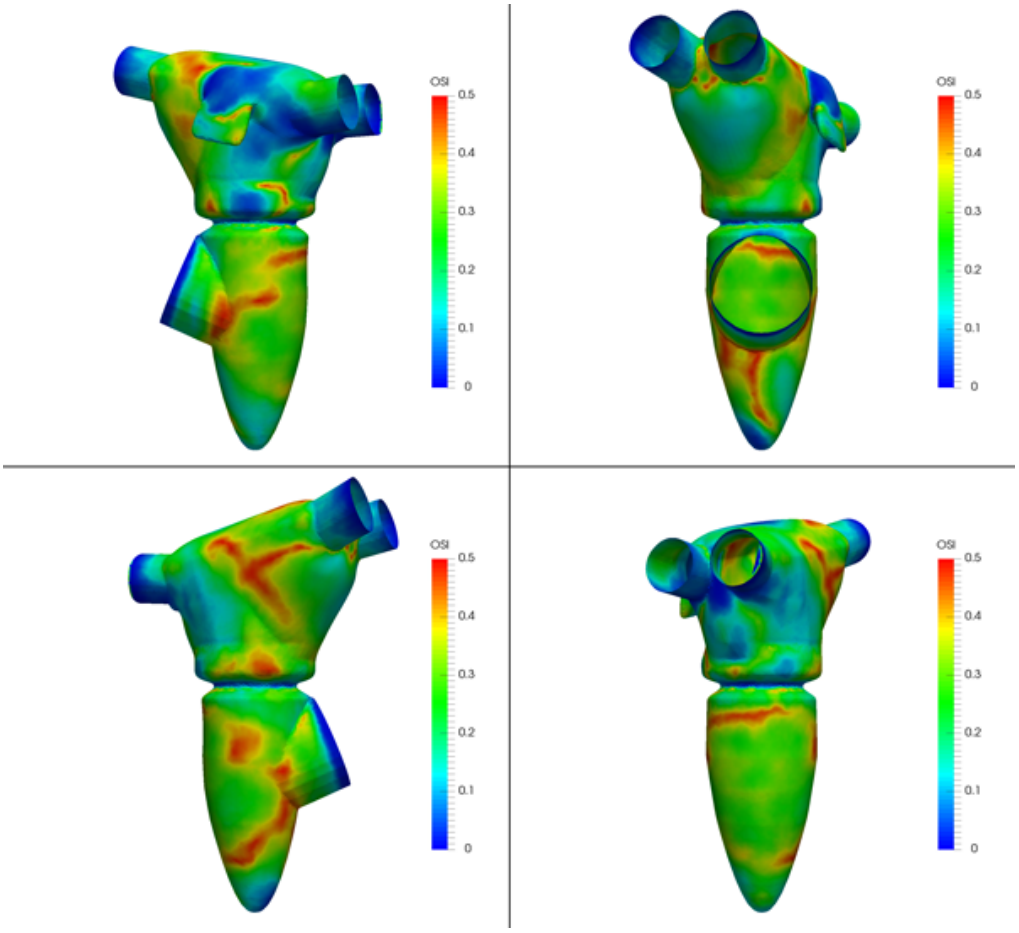


**FIGURE 13** Phase averaged Oscillatory Shear Index $\overline{OSI}$ computed by using the VMS-LES formulation

Several other indicators have been introduced to assess conditions of patients, especially for blood flows in arteries and vessels[6,54]. In this work, we report the Oscillatory Shear Index (OSI) and the Relative Residence Time (RRT) which are both based on the evaluation of the phase averaged Wall Shear Stress ($\overline{WSS}$). These are defined, respectively, as:

$$\overline{OSI} = 0.5\left(1 - \frac{\left|\int_0^T \overline{WSS}\, dt\right|_2}{\int_0^T \left|\overline{WSS}\right|_2 dt}\right), \tag{32}$$

$$\overline{RRT} = \left[\frac{(1 - 2\,\overline{OSI})}{T}\left|\int_0^T \overline{WSS}\, dt\right|_2\right]^{-1}, \tag{33}$$

where $|\cdot|_2$ denotes the Euclidean modulus of a vector.

The OSI is mostly used in arteries when studying the deposition of plaques that can lead to stenosis formation or atherosclerosis. It has been suggested that the OSI can be a valuable indicator of the locations where the deposition of material is more likely to happen in arteries[6] and possibly at the endocardium of the heart. In this respect, we remark that our idealized model neglects trabeculations of the left ventricle and atrium, for which our assessment of OSI may not indicative of thrombus formation. Rather, without necessarily relating the OSI to some specific pathological condition, we deem this indicator to be useful for a more detailed characterization of the blood flows in the left heart. In Figure 13, we report the OSI computed using the WSS based on the phase averaged velocity by means of the VMS-LES formulation. The OSI is larger in the LA at the opposite wall with respect to the LAA; in the LV, it shows non symmetric features.

The RRT is an indicator of how much time a blood particle spends in the vicinity of a wall, so it can be linked to a weak blood turnover in the regions where RRT is large, especially for flows in arteries and vessels[54]. In Figure 14, the RRT is shown. This

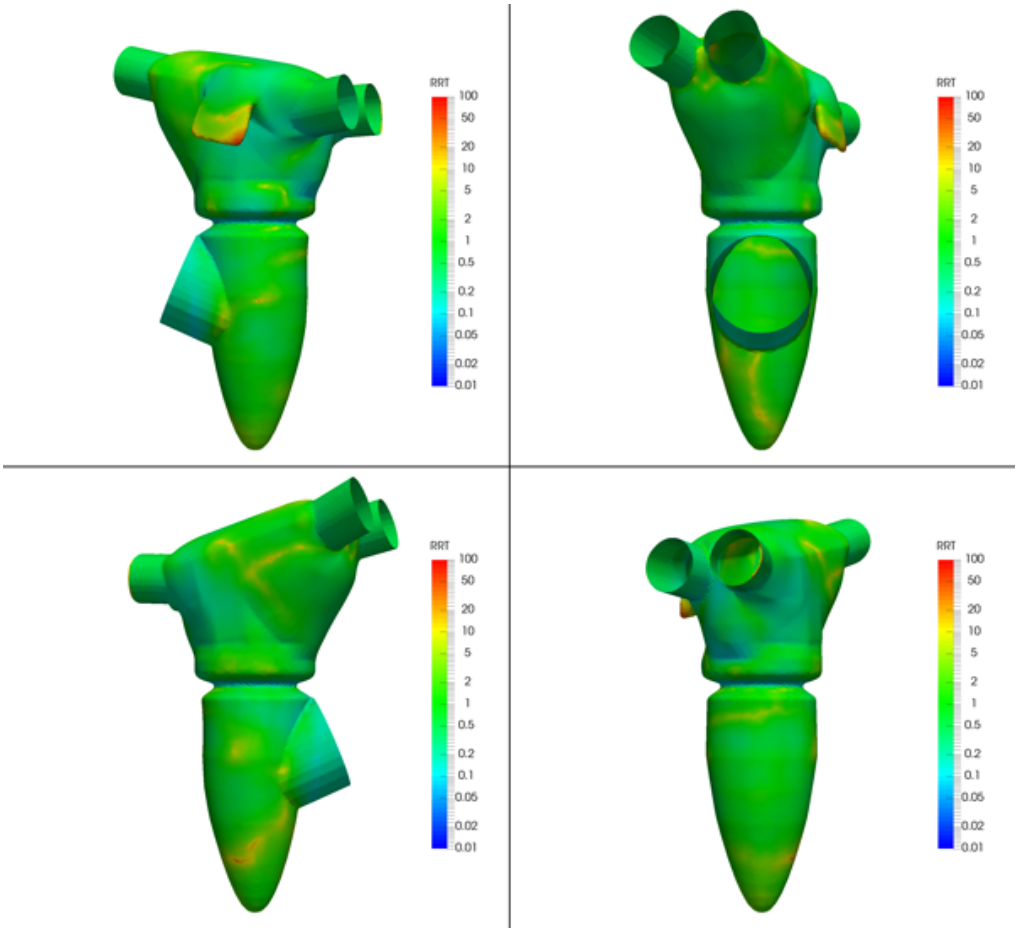


**FIGURE 14** Phase averaged Relative Residence Time $\overline{RRT}$ computed by using the VMS-LES formulation

indicator exhibits a quite uniform distribution; however, few spots where it is very large, namely in the LAA and in the LV apex, are also highlighted. In particular, the very limited washout in the LAA has been already confirmed by calculating blood particle residence time from simulations in patient-specific geometries of the LA [21,23]. Blood clotting is indeed more keen to develop in regions where washout is limited, and the RRT indicator seems to relate to these situations even for blood flows in the heart.

## 3.3 | Mitral valve regurgitation

We consider now the case of a regurgitant mitral valve; this is a pathological condition that may lead to arrhythmias, hypertension, and eventually to heart failure. Clinician decision for valve repair or replacement through surgical intervention follows from the assessment of regurgitation severity that is based on color Doppler echocardiography; see e.g. [55]. Computational studies of the fluid dynamics of left heart can help shedding light of this pathology and provide detailed insights of anomalous blood flows as done e.g. in [56,57] for idealized (mock) configuration of the mitral valve orifice.

For the numerical simulation of mitral valve regurgitation, we use the same setting and data for the idealized model that we previously illustrated. However, in this case, we virtually generate the regurgitant orifice of the mitral valve by suitably modifying the resistance function $R_h$ to account for the "hole" giving rise to this pathological scenario. A similar approach based on the resistive method was considered in [58]. The numerical simulations are performed with the VMS-LES formulation, but on a coarser mesh with about 500′000 mesh elements.

Figure 15 highlights the numerical results obtained in terms of blood flow velocity with a circular regurgitant orifice centered in the mitral valve and with an area corresponding to the 5% of the full mitral valve orifice. The results show that significantly large values of the velocity magnitude are obtained in the regurgitant orifice, as well as in the LA for most of the LV systole. In particular, this anomalous blood flow reaches and sustains peak values of the velocity magnitude around or beyond 120 cm/s,

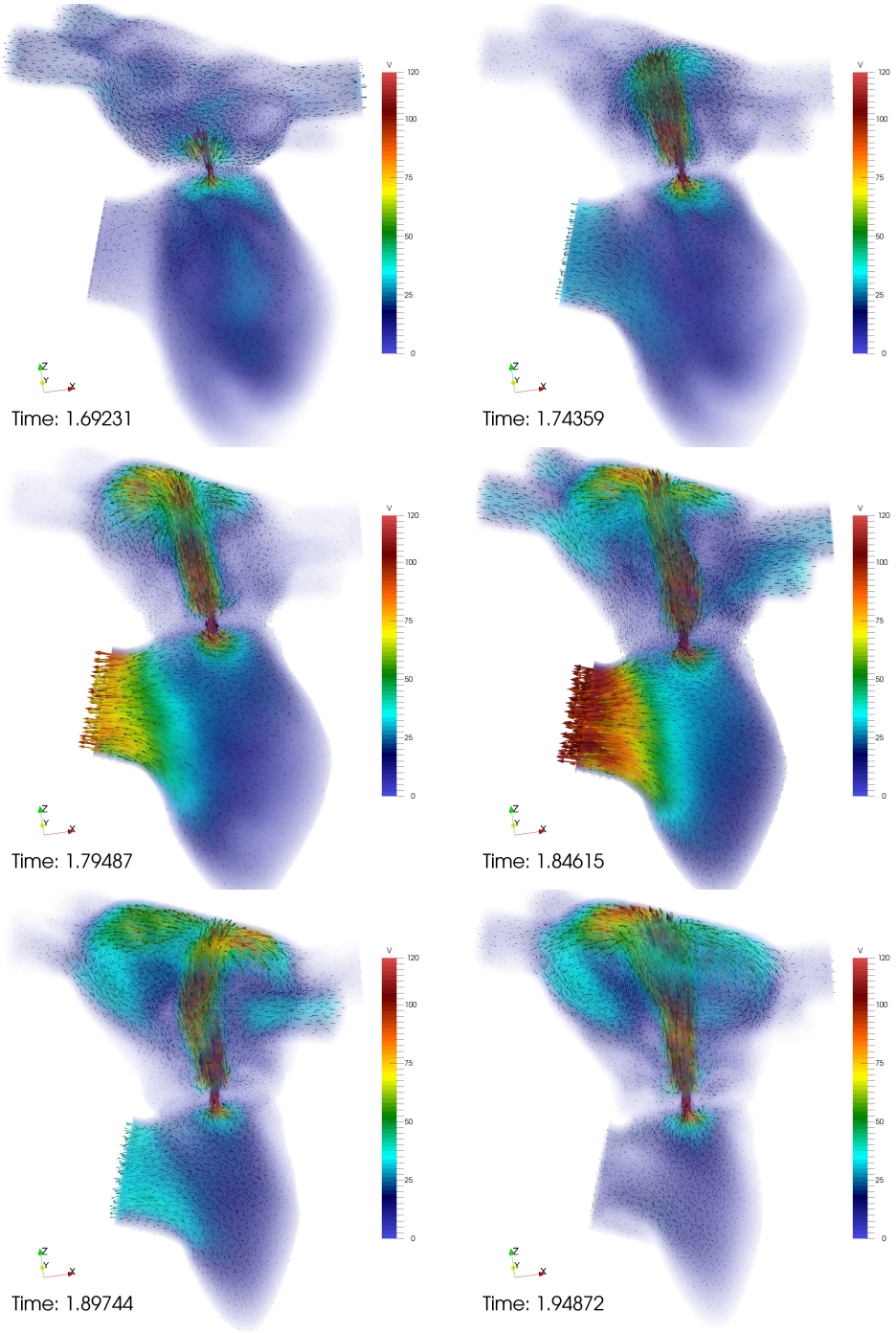


**FIGURE 15** Mitral valve regurgitation: snapshots of the velocity field and volume rendering in the LH at different time instants during systole (second heartbeat); red color corresponds to velocity magnitude around or above 120 cm/s

which are comparable and larger than those occurring across the aortic valve and in the aortic root. A strong jet impingement on the LA wall is also highlighted for most of the systolic phase. Transition to turbulence and anomalous turbulent structures develop and sustain in the LA for about 0.2 s during LV systole.

# 4 | CONCLUSIONS

In this work, we performed a numerical study of the blood flow dynamics in the left heart chambers of the human heart. Specifically, we provided a characterization of the blood flow in the left atrium and left ventricle in "normal" physiological conditions for an idealized geometry. We considered a computational model based on the incompressible Navier-Stokes equations in ALE formulation together with the resistive method to model the effect of mitral and aortic valves on the blood flow. We considered a VMS-LES formulation to account for turbulence in the flow, as well the standard SUPG stabilization technique in combination with the Finite Element approximation of the problem. The problem is defined in a moving computational domain with prescribed motion of the endocardium walls inferred by the Wiggers diagram according to physiological conditions.

We analyzed and post-processed the results of the simulations to obtain clinically meaningful fluid dynamics indicators and we critically discussed them. Among several quantitative indications and characterization of the blood flow in the left heart, the numerical results confirm that transition to turbulence is more likely to occur after the E-wave in diastole, being initiated by the breakup of the large vortex structures in the left ventricle; a similar, but less evident, situation occurs in the left atrium. Fully developed turbulence however does not appear in physiological conditions; hence, the numerical results obtained by the standard SUPG stabilization and the VMS-LES formulation are very similar, provided that space resolution is adequate. Nevertheless, the VMS-LES model provides an overall detailed description of the blood flow in the left heart and we suggest that it can be employed in the future for parametric studies across population. Indeed, in cases deviating from physiological conditions, the flow is likely to exhibit turbulence for which suitable LES modeling may be required to account for the unresolved scales of the blood flow.

We also have shown that our idealized model can be straightforwardly used to assess the pathological scenario of mitral valve regurgitation by simply modifying the resistive term according to the desired size of the regurgitant valve orifice. Albeit we did not investigate the physiology of mitral valve regurgitation nor its mechanism, this study indicates that our approach allows addressing pathological scenarios in a virtual fashion, thus making the computational pipeline a viable tool in support of medical decisions.

We are conscious that our idealized computational model presents some limitations that we intend to better address in future work. The major one is represented by treating the valve leaflets as barriers in the computational domain; in particular, our simplified assumption for the mitral valve, which neglects its bi-leaflet configuration, can drive the blood flow to the apex rather than orienting it towards the myocardium wall during the LV filling phase, thus modifying the physiological vortex ring distribution. Alternative and more detailed approaches would be the one used in [30,58], which considers different open and closed valve configurations, and that in [12] that uses moving immersed surfaces in the framework of the resistive method. A further limitation in the current model is the following: albeit the prescribed wall motion is physiologically meaningful and compliant with the Wiggers diagram, some effects like twisting of the left ventricular wall are neglected for simplicity. Also, we consider here the blood as a Newtonian fluid; given the large variability of the flow conditions along the heartbeat and the large presence of shear flows in the heart chambers, this assumption can be seen as a limitation that can be addressed by combining non–Newtonian models with the VMS–LES formulation to account for turbulence effects. We also remark that our idealized model aims at representing a "normal" heart in physiological conditions, which does not necessarily correspond to a real heart. Blood flow characterization depends on several factors, parameters, and conditions: when these vary within the physiological range (inter– and intra–patient variability), blood flow can differ by still remaining "normal". Hence, a suitable sensitivity analysis to parameters should be carried out for a full characterization of blood flows in a "normal" left heart.

A future development of our computational model is its straightforward extension to the assessment of blood flows in patient–specific cases, similarly to [22] and [21,59] for the left atrium. Here, the wall displacement would be registered for example from MRI images of the left heart and can provide a useful tool to evaluate blood flows in pathological conditions.

## Acknowledgements

The first and third authors acknowledge the ERC Advanced Grant *iHEART*, "An Integrated Heart Model for the simulation of the cardiac function", 2017–2022, P.I. A. Quarteroni (ERC–2016–ADG, project ID: 740132).

## References


1. Carlsson M, Heiberg E, Töger J, and Arheden H. Quantification of left and right ventricular kinetic energy using four-dimensional intracardiac magnetic resonance imaging flow measurements. *American Journal of Physiology: Heart and Circulatory Physiology* 2012; 302(4): 893-900.

2. Kanski M, Arvidsson P, Töger J, Borgquist R, Heiberg E, Carlsson M, and Arheden H. Left ventricular fluid kinetic energy time curves in heart failure from cardiovascular magnetic resonance 4D flow data. *Journal of Cardiovascular Magnetic Resonance* 2015; 17: 111.

3. Kawel-Boehm N, Maceira A, Valsangiacomo-Buechel ER, Vogel-Claussen J, Turkbey EB, Williams R, Plein S, Tee M, Eng J, and Bluemke DA. Normal values for cardiovascular magnetic resonance in adults and children. *Journal of Cardiovascular Magnetic Resonance* 2015; 17: 29.

4. Cimino S, Pedrizzetti G, Tonti G, Canali E, Petronilli V, De Luca L, Iacoboni C, and Agati L. In vivo analysis of intraventricular fluid dynamics in healthy hearts. *European Journal of Mechanics - B/Fluids* 2012; 35: 40-46.

5. Markl M, Frydrychowicz A, Kozerke S, Hope M, and Wieben O. 4D Flow MRI. *Journal of Magnetic Resonance Imaging* 2012; 36(5): 1015-1036.

6. Ku DN, Giddens DP, Zarins CK, and Glagov S. Pulsatile flow and athero-sclerosis in the human carotid bifurcation. Positive correlation between plaque location and low oscillating shear stress. *Arteriosclerosis* 1985; 5: 293-302.

7. Formaggia L, Quarteroni A, and Veneziani A. *Cardiovascular Mathematics: Modeling and Simulation of the Circulatory System*. Springer, 2009.

8. Quarteroni A, Dedè L, Manzoni A, Vergara C. *Mathematical Modelling of the Human Cardiovascular System. Data, Numerical Approximation, Clinical Applications*. Cambridge University Press, 2019. ISBN: 978-1108480390.

9. Quarteroni A, Lassila T, Rossi S, and Ruiz-Baier R. Integrated Heart - Coupling multiscale and multiphysics models for the simulation of the cardiac function. *Computer Methods in Applied Mechanics and Engineering* 2017; 314: 345-407.

10. Sugiura S, Washio T, Hatano A, Okada J, Watanabe H, and Hisada T. Multi-scale simulations of cardiac electrophysiology and mechanics using the University of Tokyo heart simulator. *Progress in Biophysics and Molecular Biology* 2012; 110: 380-389.

11. Gerbi A, Dedè L, and Quarteroni A. A monolithic algorithm for the simulation of cardiac electromechanics in the human left ventricle. *Mathematics in Engineering* 2018; 1(1): 1-37.

12. Fedele M, Faggiano E, Dedè L, and Quarteroni A. A patient-specific aortic valve model based on moving resistive immersed implicit surfaces. *Biomechanics and Modeling in Mechanobiology* 2017; 16(5): 1779-1803.

13. Nobili M, Morbiducci U, Ponzini R, Gaudio CD, Balducci A, Grigioni M, Montevecchi FM, and Redaelli A. Numerical simulation of the dynamics of a bileaflet prosthetic heart valve using a fluid-structure interaction approach. *Journal of Biomechanics* 2008; 41: 2539-2550.

14. Tricerri P, Dedè L, Gambaruto A, Quarteroni A, and Sequeira A. A numerical study of isotropic and anisotropic constitutive models with relevance to healthy and unhealthy cerebral arterial tissues. *International Journal of Engineering Science* 2016; 101: 126-155.

15. Sacks MS, Merryman WD, and Schmidt DE. On the biomechanics of heart valve function. *Journal of Biomechanics* 2009; 42: 1804-1824.

16. De Tullio MD, Cristallo A, Balaras E, and Verzicco R. Direct numerical simulation of the pulsatile flow through an aortic bileaflet mechanical heart valve. *Journal of Fluid Mechanics* 2009; 622: 259-290.

17. Griffith BE. Immersed boundary model of aortic heart valve dynamics with physiological driving and loading conditions. *International Journal for Numerical Methods in Biomedical Engineering* 2012; 28(3): 317-345.

18. Tagliabue A. *Mathematical and Numerical Modeling of Blood Flow in an Idealized Left Ventricle*. PhD Thesis. Politecnico di Milano; 2016.

19. Tagliabue A, Dedè L, and Quarteroni A. Fluid dynamics of an idealized left ventricle: the extended Nitsche's method for the treatment of heart valves as mixed time varying boundary conditions. *International Journal for Numerical Methods in Fluids* 2017; 85(3): 135-164.

20. Tagliabue A, Dedè L, and Quarteroni A. Complex blood flow patterns in an idealized left ventricle: A numerical study. *Chaos* 2017; 27: 093939.

21. Masci A, Alessandrini M, Forti D, Menghini F, Dedè L, Tommasi C, Quarteroni A, and Corsi C. A patient-specific computational fluid dynamics model of the left atrium in atrial fibrillation: development and initial evaluation. In: Pop M and Wright G (eds), Functional Imaging and Modelling of the Heart. FIMH 2017. Lecture Notes in Computer Science, Springer, Cham, 2017; 10263: 392-400.

22. Chafna C, Mendez S, and Nicoud F. Image based Large-Eddy Simulation in a realistic left heart. *Computers & Fluids* 2014; 94: 173-187.

23. Koizumi R, Funamoto K, Hayase T, Kanke Y, Shibata M, Shiraishi Y, and Yambe T. Numerical analysis of hemodynamic changes in the left atrium due to atrial fibrillation. *Journal of Biomechanics* 2015; 48: 472-478.

24. Blanco PJ and Feijoo RA. A 3D-1D-0D computational model for the entire cardiovascular system. *Mecanica Computacional* 2010; XXIX:5887-5911.

25. Hirschvogel M, Bassilious M, Jagschies L, Wildhirt SM, and Gee MW. A monolithic 3D-0D coupled closed-loop model of the heart and the vascular system: Experiment-based parameter estimation for patient-specific cardiac mechanics. *International Journal of Numerical Methods in Biomedical Engineering* 2017; 33:e2842.

26. Korakianitis T and Shi Y. Numerical simulation of cardiovascular dynamics with healthy and diseased heart valves. *Journal of Biomechanics* 2006; 39: 1964-1982.

27. Colciago CM, Deparis S, and Quarteroni A. Comparisons between reduced order models and full 3D models for fluid-structure interaction problems in hemodynamics. *Journal of Computational and Applied Mathematics* 2014; 265: 120-138.

28. Quarteroni A, Manzoni A, and Negri F. *Reduced Basis Methods for Partial Differential Equations. An Introduction.* 92. Springer, Unitext Series 2015.

29. Wiggers C. *Circulation in Health and Disease*. Lea & Febiger, Philadelphia, 1915.

30. Astorino M, Hamers J, Shadden SC, and Gerbeau JF. A robust and efficient valve model based on resistive immersed surfaces. *International Journal of Numerical Methods in Biomedical Engineering* 2012; 28(9): 937-959.

31. Fernández MA, Gerbeau JF, and Martin V. Numerical simulation of blood flows through a porous interface. *ESAIM Mathematical Modeling and Numerical Analysis* 2008; 42(06): 961-990.

32. Domenichini F, Pedrizzetti G, and Baccani B. Three-dimensional filling flow into a model left ventricle. *Journal of Fluid Mechanics* 2005; 539: 179-198.

33. Pedrizzetti G and Domenichini F. Nature optimizes swirling flow in the human left ventricleâĂİ. *Physical Review Letters* 2005. 95: 108101.

34. Vedula V, Seo JH, Lardo AC, and Mittal R. Effect of trabeculae and papillary muscles on the hemodynamics of the left ventricle. *Theoretical and Computational Fluid Dynnamics* 2014; 1-19.

35. Watanabe H, Sugiura S, Kafuku H, and Hisada T. Multiphysics simulation of left ventricular filling dynamics using fluid-structure interaction finite element method. *Biophysics Journal* 2004; 87: 2074âĂŞ2085.

36. Mittal R, Seo JH, Vedula V, Choi YJ, Liu H, Huang HH, Saurabh J, Younes L, Abraham T, and George RT. Computational modeling of cardiac hemodynamics: current status and future outlook. *Journal of Computational Physics* 2016; 305: 1065-1082.

37. Zheng X, Seo JH, Vedula V, Abraham T, and Mittal R. Computational modeling and analysis of intracardiac flows in simple models of the left ventricle. *European Journal of Mechanics – B/Fluids* 2012; 35: 31-39.

38. Pope SB. Ten questions concerning the large-eddy simulation of turbulent flows. *New Journal of Physics* 2004; 6(35).

39. Germano M, Piomelli U, Moin P, and Cabot WH. A dynamic subgrid-scale eddy viscosity model. *Physics of Fluids* 1991; 3(7).

40. Bazilevs Y, Calo VM, Cottrell JA, Hughes TJR, Reali A, and Scovazzi G. Variational multiscale residual-based turbulence modeling for Large Eddy Simulation of incompressible flows. *Computer Methods in Applied Mechanics and Engineering* 2007; 197: 173-201.

41. Doost SN, Zhong L, Su B, and Morsi YS. The numerical analysis of non-Newtonian blood flow in human patient-specific left ventricle. *Computer Methods and Programs in Biomedicine* 2016, 127: 232-247.

42. Johnson AA and Tezduyar TE. Mesh update strategies in parallel finite element computations of flow problems with moving boundaries and interfaces. *Computer Methods in Applied Mechanics and Engineering* 1994; 119: 73-94.

43. Forti D and Dedè L. Semi-implicit BDF time discretization of the Navier-Stokes equations with VMS-LES modeling in a High Performance Computing framework. *Computers & Fluids* 2015; 117: 168-182.

44. Patelli AS, Dedè L, Lassila T, Bartezzaghi A, and Quarteroni A. Isogeometric approximation of cardiac electrophysiology models on surfaces: an accuracy study with application to the human left atrium. *Computer Methods in Applied Mechanics and Engineering* 2017; 317: 248-273.

45. Menghini F, Dedè L, Forti D, and Quarteroni A. Hemodynamics in a left atrium based on a Variational Multiscale-LES numerical model. *MOX report* 47/2017, Politecnico di Milano: 2017.

46. Korhonen M, Parkkonen J, Hedman M, Muuronen A, Onatsu J, Mustonen P, Vanninen R, and Taina M. Morphological features of the left atrial appendage in consecutive coronary computed tomography angiography patients with and without atrial fibrillation. *PLoS ONE* 2017; 12(3).

47. Hsu MC, Kamensky D, Bazilevs Y, Sacks MS, and Hughes TJR. Fluid-structure interaction analysis of bioprosthetic heart valves: significance of arterial wall deformation. *Computational Mechanics* 2014; 54(4): 1055-1071.

48. Bazilevs Y, Calo VM, Hughes TJR, and Zhang Y. Isogeometric fluid-structure interaction: theory, algorithms and computations. *Computational Mechanics* 2008; 43: 3-37.

49. Bazilevs Y, Gohean JR, Hughes TJR, Moser RD, and Zhang Y. Patient-specific Isogeometric fluid-structure interaction analysis of thoracic aortic blood flow due to implantation of the Jarvik 2000 left ventricular assist device. *Computer Methods in Applied Mechanics and Engineering* 2009; 198: 3534-3550.

50. Quarteroni A, Veneziani A, and Vergara C. Geometric multiscale modeling of the cardiovascular system, between theory and practice. *Computer Methods in Applied Mechanics and Engineering* 2016; 302: 193-252.

51. LifeV website: <www.lifev.org>.

52. Umeki M. Numerical simulation of plane Poiseuille turbulence. *Fluid Dynamics Research* 1994; 13: 67-79.

53. Lupo AR, Mokhov II, Dostoglou S, Kunz AR, and Burkhardt JP. Assessment of the Impact of the Planetary Scale on the Decay of Blocking and the Use of Phase Diagrams and Enstrophy as a Diagnostic. *Izvestiya, Atmospheric and Oceanic Physics* 2007; 43(1): 45-51.

54. Himburg HA, Grzybowski DM, Hazel AL, LaMack JA, Li XM, and Friedman MH. Spatial comparison between wall shear stress measures and porcine arterial endothelial permeability. *American Journal of Physiology: Heart and Circulatory Physiology* 2004; 286: 1916-1922.

55. Little SH, Pirat B, Kumar R, Igo SR, McCulloch M, Hartley CJ, Xu J, and Zoghbi WA. Three-dimensional color Doppler echocardiography for direct measurement of vena contracta area inmitral regurgitation: in vitro validation and clinical experience. *JACC Cardiovascular Imaging* 2008; 1:695-704.

56. Quaini A, Canic S, Guidoboni G, Glowinski R, Igo Sr, Hartley CJ, Zoghbi, WA, and Little SH. A three-dimensional computational fluid dynamics model of regurgitant mitral valve flow: validation against in vitro standards and 3D color Doppler methods. *Cardiovascular Engineering and Technology* 2011; 2(2): 77-89.

57. Wang Y, Quaini A, Canic S, Vukicevic M, and Little SH. 3D experimental and computational analysis of eccentric mitral regurgitant jets in a mock imaging heart chamber. *Cardiovascular Engineering and Technology* 2017; 8: 419-438.

58. This A, Boilevin-Kayl L, Morales HG, Bonnefous O, Allain P, Fernández MA, and Gerbeau JF. One mesh to rule them all: registration-based personalized cardiac flow simulations. In: Pop M and Wright G (eds), Functional Imaging and Modelling of the Heart. FIMH 2017. Lecture Notes in Computer Science, Springer, Cham, 2017; 10263: 441-449.

59. Masci A, Barone L, Dedè L, Fedele M, Tomasi C, Quarteroni A, and Corsi C. The impact of left atrium appendage morphology on stroke risk assessment in atrial fibrillation: a computational fluid dynamics study. *Frontiers in Physiology* 2019; 9: 1938.